LANTHANUM DOPED CALCIUM SILICATE NANOPARTICLES FOR DRUG DELIVERY AND X-RAY CONTRAST IMAGING

2021
MASTER THESIS
DEPARTMENT OF BIOMEDICAL ENGINEERING

Youssouf Abakar ADAM

THESIS ADVISOR
Assist. Prof. Dr. Ammar Zeidan Ghailan ALSHEMARY

LANTHANUM DOPED CALCIUM SILICATE NANOPARTICLES FOR DRUG DELIVERY AND X-RAY CONTRAST IMAGING

Youssouf Abakar ADAM

T.C.
Karabük Üniversitesi
Institute of Graduate Programs
Department of Biomedical Engineering
Prepared as Master Thesis

Thesis Advisor
Assist Prof. Dr. Ammar Zeidan Ghailan ALSHEMARY

KARABÜK
December 2021

I certify that in my opinion the thesis submitted by Youssouf Abakar ADAM titled "LAMTHANUM DOPED CALCIUM SILICATE NANOPARTICLES FOR DRUG DELIVERY AND X-RAY CONTRAST IMAGING" is fully adequate in scope and in quality as a thesis for the degree of Master of Science.

Assist. Prof. Dr. Ammar Zeidan Ghailan ALSHEMARY .....
Thesis Advisor, Department of Biomedical Engineering

This thesis is accepted by the examining committee with a unanimous vote in the Department of Biomedical Engineering as a Master of Science thesis. December 10, 2021.

Examining Committee Members (Institutions)	Signature
Chairman: Prof. Dr. Fatma KANDEMIRLI (KU)	Online
Member: Assist.Prof.Dr. Ammar Zeidan Ghailan ALSHEMARY (KBU)	.....
Member: Assist. Prof. Dr. Hacı Mehmet KAYILI (KBU)	.....

The degree of Master of Science by the thesis submitted is approved by the Administrative Board of the Institute of Graduate Programs, Karabuk University.

Prof. Dr. Hasan SOLMAZ .....
Director of the Institute of Graduate Programs

"I hereby declare that all information in this document has been obtained and presented in accordance with academic rules and ethical conduct. I also declare that, as required by these rules and conduct, I have fully cited and referenced all material and results that are not original to this document."

Youssouf Abakar ADAM

ABSTRACT

M.Sc. Thesis

LANTHANUM DOPED CALCIUM SILICATE NANOPARTICLES FOR DRUG DELIVERY AND X-RAY CONTRAST IMAGING

Youssouf Abakar ADAM

Karabük University
Institute of Graduate Programs
Department of Biomedical Engineering

Thesis Advisor:
Assist. Prof. Dr. Ammar Zeidan Ghailan ALSHEMARY
December 2021, 84 pages

Bioceramics are a kind of material used to heal or replace damaged bone tissues. Bioceramics may enhance tissue development or induce new tissue regeneration when utilized in combination with bioactive ceramics, depending on the application. In this study, pure phase of Calcium silicates (CS) doped with different fractions of lanthanum (La^{3+}) (0, 5, 10, and 20 %) were successfully prepared using the wet precipitation method. The impact addition of La^{3+} ions was evaluated using X-ray powder diffraction (XRD), Fourier transform infrared spectroscopy (FTIR), X-ray photoelectron spectroscopy (XPS), Scanning electron microscope (SEM), Surface area (Brunauer, Emmett and Teller, BET), and Thermogravimetric analysis (TGA). With the incorporation of La^{3+} ions, it was observed that the diffraction peaks were shifted to the high value of theta, the vibration bands of the SiO_3 group were shrinkage, the binding energy of La^{3+} ions was detected in the range of 831-852 eV, the particles existed irregular morphology shapes and non-uniform microcrystalline

particles, the surface area decreased from 9.742 m^2g^{-1} for CS to 2.12 m^2g^{-1} for the La-CS (20% of La^{3+}). The radiopacity of composites was evaluated using an x-ray machine. The incorporation of La^{3+} ions into CS significantly improved the contrast of the radiographic images. The *in vitro* drug (Gentamicin sulphate, Cephalexin hydrate, and Ampicillin sodium) delivery and release was investigated for 3 days. The results showed that with the increase of La^{3+} ions up to 20% into the structure of CS, the loading rate of Ampicillin sodium was increased from 1.150 mg to 1.202 mg, the loading rate of Cephalexin hydrate was decreased from 0.55 mg to 0.46 mg, and the loading rate of Gentamicin sulphate was increased from 0.120 mg to 0.224 mg. The release profile of antibiotics was sustained over the immersion period. The obtained materials in this study have the potential to use as a carrier vehicle for wide ranges of antibiotics.

Keywords **:** Calcium silicate, Lanthanum, characterizations, radiographic imaging, drug delivery.

Science code **:** 92503

ÖZET

Yüksek Lisans Tezi

İLAÇ SALIMI VE X-RAY KONTRAST GÖRÜNTÜLEME İÇİN NANOPARTİKÜL LANTANUM KATKILI KALSİYUM SİLİKAT

Youssouf Abakar ADAM

Karabük Üniversitesi
Lisansüstü Eğitim Enstitüsü
Biyomedikal Mühendisliği Anabilim Dalı

Tez Danışmanı:
Dr. Öğr. Üyesi Ammar Zeidan Ghailan ALSHEMARY
Aralık 2021, 84 sayfa

Biyoseramik, hasarlı kemik dokularını iyileştirmek veya değiştirmek için kullanılan bir tür malzemedir. Uygulamaya bağlı olarak, biyoaktif seramikle birlikte kullanıldığında doku büyümesini veya yeni doku rejenerasyonunu teşvik edebilir. Bu çalışmada, farklı lantan (La^{3+}) (0, 5, 10 ve 20 %) ile katkılı kalsiyum silikatların (CS) saf fazı yaş çöktürme yöntemiyle başarıyla hazırlandı. La^{3+} iyonlarının ilavesinin etkisi, X-ışını kırınımı (XRD), fourier dönüşümlü kızılötesi spektroskopisi (FTIR), X-ışını fotoelektron spektroskopisi (XPS), taramalı elektron mikroskobu (SEM), yüzey alanı (Brunauer, Emmett Teller, BET) ve termogravimetrik analiz (TGA) yöntemleri kullanılarak değerlendirildi. La^{3+} iyonlarının dâhil edilmesiyle, kırınım piklerinin yüksek teta değerine kaydığı, SiO_3 grubunun titreşim bantlarının küçüldüğü, La^{3+} iyonlarının bağlanma enerjisinin 831-852 eV aralığında olduğu, partiküllerin düzensiz morfoloji şekillerine ve düzgün olmayan mikrokristal partiküllerini içerdiği, yüzey alanının CS için 9.742 m^2g^{-1}'den La-CS için 2.12 m^2g^{-}

[1]'e düştüğü belirlendi (La^{3+}'ın %20'si). Kompozitlerin radyoopasitesi bir x-ray cihazı kullanılarak değerlendirildi. La^{3+} iyonlarının CS'ye dâhil edilmesi, radyografik görüntülerin kontrastını önemli ölçüde iyileştirdi. *İn vitro* ilaç (Gentamisin sülfat, Cephalexin hidrat ve Ampisilin sodyum) taşınımı ve salınımı 3 gün boyunca incelendi. Sonuçlar, CS yapısına La^{3+} iyonlarının %20'ye kadar artmasıyla Ampisilin sodyum yükleme oranının 1.150 mg'dan 1.202 mg'a yükseldiğini, Cephalexin hidrat yükleme oranının 0.55 mg'dan 0.46 mg'a düştüğünü ve Gentamisin sülfat yükleme oranının 0.120 mg'dan 0.224 mg'a yükseldiğini göstermiştir. Antibiyotiklerin salınım profili, daldırma süresi boyunca sürdürülmüştür. Bu çalışmada elde edilen malzemeler, çok çeşitli antibiyotikler için taşıyıcı araç olarak kullanım potansiyeline sahiptir.

Anahtar Sözcükler : Kalsiyum silikat, Lantan, karakterizasyon, radyografik görüntüleme, ilaç salımı.

Bilim Kodu : 92503

ACKNOWLEDGMENT

I'd like to extend my sincerest gratitude towards. Assist. Prof. Dr. Ammar Zeidan Ghailan ALSHEMARY for accepting my request to work under his guidance, his continued support, timely interventions, and sound advice throughout the course of my project work are what lead to its eventual success. Although his nature of expecting perfection would often push me to continually improve and hone my skills, his friendly demeanor made him a guide who was easy to approach and connects with on a personal level. The warmth he showered upon me certainly instills in me a feeling that I wasn't wrong in pursuing my research under his experienced guidance.

I am extremely grateful to Assist. Prof. Dr. Mehmet KAYILI, he has been a tremendous mentor and guide for me in the lab. I would like to thank him for encouraging me to research. I would like to express my sincere gratitude and appreciation to Mr. Hossein Jodati for his assistance in the laboratory.

Especially thanks to my mother, my wife, and my brother for the support and help from my family is highly acknowledged. I would also like to thank all my friends who helped me with everything.

I also very much thank the University of Karabuk for providing financial support through Project KBÜBAP-21-YL-042.

CONTENTS

Page

LIST OF FIGURES

Page

LIST OF TABLE

Page

SYMBOLS AND ABREVIATIONS

ABBREVIATION

BET : Brunauer- Emmet- Teller

BGs : Bioglasses

$CaSO_4$: Calcium sulfate

CaSR : Calcium-sensing receptor

CP : Calcium phosphate

JCPDS : Joint Committee on Powder Diffraction and Standards

CS : Calcium silicate

FTIR : Fourier-transform infrared spectroscopy

HA : Hydroxyapatite

IBU : Ibuprofen

IUPAC : International union of pure and applied chemistry

IGF II : Insulin-like growth factor

MCM-41 : Mobil Composition of Matter41

MSCs : Mesenchymal stem cells

PBS : Phosphate Buffered Saline

PMMA : Polymethyl methacrylate

SBA-15 : Santa Barbra Amorphous-15

SBF : Simulated Body Fluid

SEM : Scanning Electron Microscopy

TCP : Tricalcium phosphate

TGA : Thermogravimetric Analysis

TiO_2 : Titanium oxide

UV : Ultraviolet

XPS : X-ray photoelectron spectroscopy

XRD : X-ray Powder Diffraction

GPa : Gega pascal

MPa : Mega pascal

AMP : Ampicillin

GEN : Gentamicin sulfate

CPA : Cephalexin hydrate

SYMBOLS

° : Degree

°C : The degree Celsius

μL : Microliter

Å : Angstrom

Cm : Centimeter

nm : Nanometer

2θ : The diffraction angle

h : Hours

gr : Gram

CHAPTER 1

INTRODUCTION

1.1. OVERVIEW

Bone is a specialized connective tissue, has three main functions: a scaffold that muscle attachment for movement, protects vital organs and soft tissues, furthermore, it contains a stock of ions, especially Ca^{2+} and phosphate ions, one of its unique characteristics is its ability to undergo constant reconstruction even after the growth and modelling of the skeleton have been completed. This process enables the bone to respond and adapt to changing functional situations [1, 2]. In addition, it houses the production of blood cells, minerals, and growth factors. It also plays an important role in detoxification and acid-base balance [3]; however, the bone is generally an organ with poor blood circulation compared to the rest of the body [4-6]. The bone tissues are composed of cells separated by an intercellular substance (mature bone cells that maintain the bone matrix), which consists of (i) osteoblasts, which are bone-producing cells (immature bone cells secreting the organic components of the matrix). (ii) Osteoclasts are bone-removing cells (a multinucleate cell, which secretes acids and enzymes that dissolve bone). Once resorption is complete, the osteoclasts stop producing and become inactive for a period [7]. (iii) osteoprogenitor cells from which are derived osteoblasts and osteoclasts (these are stem cells) [6, 8]. Bones have endocrine function, mechanical support and protection, mineral homeostasis, and hematopoiesis [9]. Bones are generally composed of organic and inorganic materials. The organic part is made up of collagen (90%), proteoglycans (10%), growth factors, and cytokines [10]. The inorganic part are mainly composed of hydroxyapatite (HA). It is about 2-10 nm thick, 20-50 nm long, and more than 15-30 nm wide [11-13]. HA is formed in human bones with ionic substitutes such as CO_3^{2-} or Na, Sr^{2+}, Mg^{2+}, K^+ [14]. There are two types of bone, cortical, and trabecular bone. Cortical bone comprises about

80% of total bone mass. It is a dense bone layer, which forms the outer covering of all bones. The trabecular bone represents only 20% of total bone mass. it is a very complex network. It's found within the cortical bone layer. It's penetrated by other tissues such as the bone marrow, blood vessels and nerves [15]. The first step to form new bone is the emergence of a thin layer of collagen. It is a layer that contains mucopolysaccharides and contains a high percentage of Ca^{2+} [7]. Second step: secreted osteoid osteoblasts traps, which then become osteocytes, third step: the trabecular matrix and the periosteum form, and fourth step: the compact bone develops superficially to the trabecular bone, and congested blood vessels condense into red marrow [16].

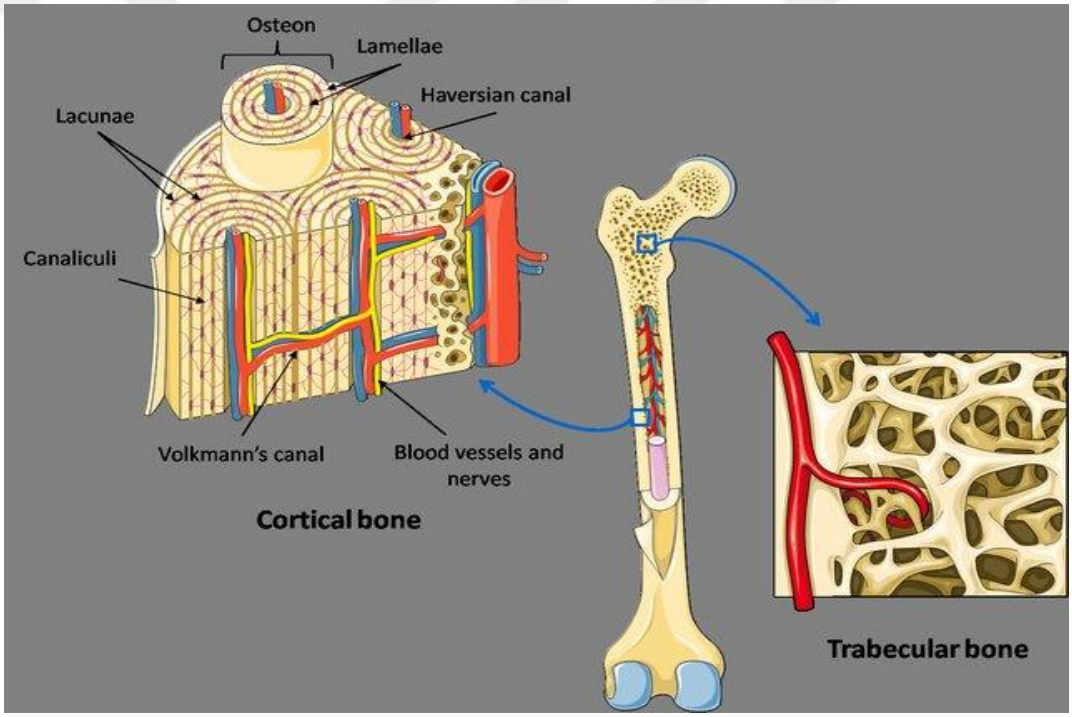

Figure 1.1. Hierarchical organization showing different bone structures [17].

Bone modelling: occurs primarily when bone resorption and formation occur on different surfaces, i.e., Formation and resorption are two opposite processes that are not coupled. From birth to adulthood, the long bones are constantly growing in both diameter and length. It is responsible for increasing the mass of the skeleton and changes in the shape of the skeleton [18].

Bone remodelling: It is a process that usually occurs mainly in adults to maintain bone mass. It has five stages: (i) Activation: occurring under the influence of cytokines and growth factors. The former pre-osteoclasts are usually stimulated and differentiated into mature active osteoclasts. (ii) Resorption: it is the digestion of the mineral matrix of old bone after the formation of new bone and after producing an acidic environment in the medium. (iii) Reflection**:** after completing the osteoclast by the apoptosis method, the pre-osteoblast activation occurs. (iv) Formation: the separation or differentiation of osteoblasts and the synthesis of new bone matrix. (v) Quiescence: at this stage, osteoblasts become cells lining the newly formed bone [19, 20].

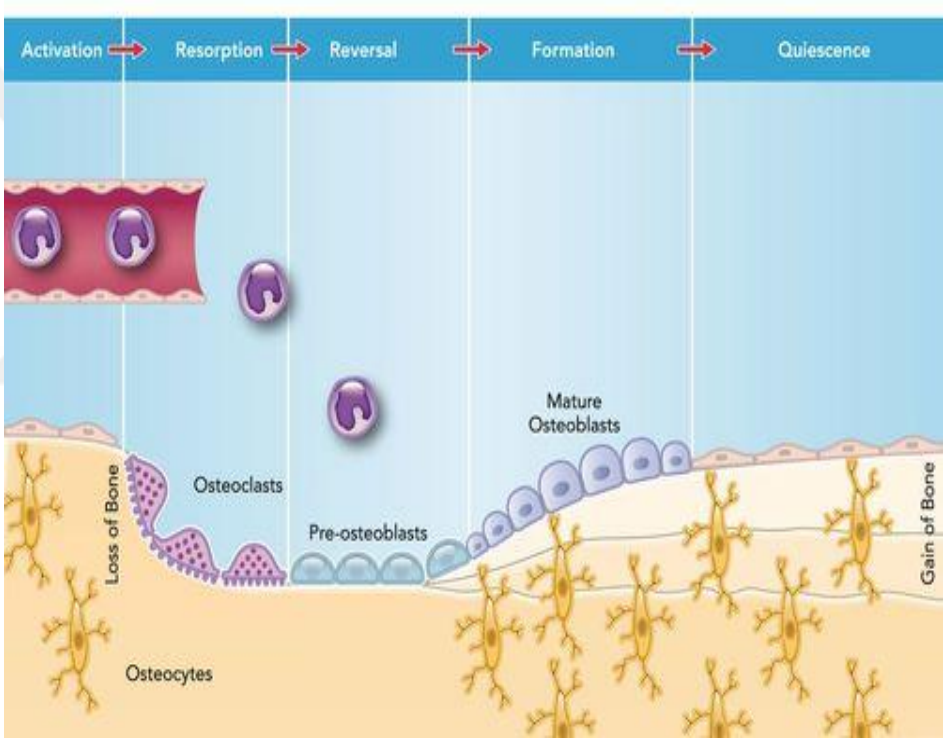

Figure 1.2. Bone remodelling process [21].

1.1.1. Bone Substitute Materials

Bone substitutes are synthetic, organic, or inorganic biological materials that can be introduced to replace, stimulate, or treat some autologous or allogeneic bone defect. There are clinical limitations that have limited the use of these materials. Currently, alternative techniques for bone repair have been developed. These developments have led to scaffold tissue engineering strategies [22]. There are several factors for

the successful incorporation of the graft material, including the graft type, vascularity, mechanical strength, and pore size. Selecting the graft materials depends on many factors (e.g., dealing with the harvest site's morbidity). Another crucial area to consider is whether the graft primarily provides fully mechanical or biological support. Individual features affect the quality of the chosen graft, its success, and the overall outcome of the surgery. There are four desirable characteristics of bone grafting materials: osteogenesis, osteoinductive, osteoconductive, and osteointegration. The grafting material containing these four features is called autologous bone, which is why it is the gold standard in bone grafting [23]. Regular bone healing depends heavily on mechanical stability, enhanced by biophysical stimulation (e.g., ultrasound, shockwave, and electromagnetic field). However, treatment of large bone defects is a significant challenge in reconstructive surgery [24].

1.1.2. Synthetic Bone Substitutes

Wide ranges of synthetic materials have been used over time to fill in bone defects. For synthetic materials to be used for bone grafting, they must possess at least two of the four essential characteristics (osteointegration, osteoconduction). They must also be biocompatible ideally and support new bone formation. From a mechanical point of view synthetic bone, materials should have similar strength as those in the cortical/cancellous bone being replaced [25].

1.1.3. Role of Calcium and in Bone Metabolisme

The human body contains 2% of Ca^{2+}, and 98% of the total Ca^{2+} is located in bones and teeth, and the remaining part is found in the body fluid. Ca^{2+} play a biological role outside the cell, independently regulating bone recovery from hormones by stimulating calcium-sensing receptors (CaSR). For example, extracellular Ca^{2+} can enhance the usefulness of insulin-like growth factor (IGF II), which explicitly regulates the proliferation of osteoblast. Also, its extracellular concentrations can improve the release of osteoblast glutamate [26]. Regulates extracellular CaSR expressed on bone cells where it regulates skeletal homeostasis. In young animals,

CaSR activate the osteoclasts to inhibit bone resorption, which leads to the promotion of bone-building. In contrast, in old animals, CaSR activates osteoblasts augment bone formation [27]. The calcium-selective channel (TRPV6) has been shown to play a role in bone metastasis [28]. Despite cytokines and other bone growth factors, Ca^{2+} is one of the critical elements in the formation of bone metastasis. It should be considered when planning therapeutic strategies to prevent bone metastasis. Conversely, Ca^{2+} can be used to avoid bone metastasis, calcium mimetic R-223 that blocks CaSR is an example of a new bone-targeted therapy with powerful anti-tumours effects [29].

Silicon (Si^{4+}) is a trace element, non-metallic, distributed in the body from 1 to 2 gr (the third most abundant element after iron and zinc). Inside the bone, Si^{4+} binds with glycosaminoglycan, the latter being the main component of the extracellular matrix (ECM) and demonstrating that Si^{4+} plays an avital role in bone structure and formation. It has a significant role in regulating cellular responses, promoting cell growth and differentiation in osteoblasts. The nature of its action varies on its quantity. For example, osteoblasts favour proliferation and differentiation when it is at a 2-4 mmol concentration. The ideal Si^{4+} ratio to mineralise the extracellular bone matrix is 6-8 mmol; when it exceeds 10 mmol showed toxic behaviour [30, 31].

Furthermore, Si^{4+} is rarely toxic when taken orally, and it is essential for the correct metabolism of connective tissues and bones. In addition, it accelerates the mineralisation process in bone by affecting collagen, inhibiting bone reabsorption in postmenopausal women [30, 31]. Zinc, copper, and manganese are essential cofactors for enzymes involved in synthesizing components of the bone matrix [32].

1.1.4. Synthetic Bioceramics for Controlled Drug Delivery

Osteomyelitis is a bone infection or an inflammatory process accompanied by bone destruction caused by infectious microorganisms [33]. Osteomyelitis often occurs after trauma, surgery. Or secondary factors that cause osteomyelitis, such as a lack of blood vessels in some part of the body to supply the bones and protect it by transporting phagocytes. Bone tissue, by its hard nature, is usually resistant to

infection. However, some factors make the bone susceptible to inflammation, such as necrosis, foreign implants, and chronic diseases e.g., diabetes [34-36]. Eid, Albert J et al. approved that the bones are highly resistant to infection, and osteomyelitis does not arise in them except when a large organic suppuration or trauma has damaged the bone or the presence of foreign materials such as poorly sterilized implants [37]. In infants: Most infections are caused by *Staphylococcus aureus* (S. aureus), *Escherichia coli* (E.coli) *Streptococcus agalactiae* (S. agalactiae) *Streptococcus pyogenes* (S.pyogenes), and *Haemophilus influenzae* (H. influenzae) [38], while in adults, (S. aureus) is the most common bacteria, despite the existence of other types of bacteria, they represent the vast majority in all age groups [39]. Overall, other pathogenic microorganisms associated with osteomyelitis include anaerobic and *mycoidal species* (especially Candida), *Enterococcus species* (spp), *Mycobacterium spp* as well as *Enterobacter spp, Pseudomonas aeruginosa, Streptococcus spp* [40, 41]. The record of 36 patients with diabetes, which in turn led to osteomyelitis, was reviewed, and samples were taken from a university hospital in Texas for the common bacteria causing osteomyelitis in these patients between January 1, 1990 and December 30, 1992. The results are summarized in Table 1.3.

Table 1.1. The bacteria causes osteomyelitis [42].

Bacterial Species		
Gram positive aerobes	Gram negative aerobes	Anaerobes
Staphylococcus aureus	*Pseudomonas aeruginosa*	*Clostridium species*
Enterococcus	*Klebsiella*	*Peptostreptococcus*
Staphylococcus epidermidis	*Proteus*	*Bacteroidies species*
Streptococcus other	*Serratia*	*Fusobacterium*
Corynebacterium	*Escherichia coli*	
	Enterobacter	
	Citrobacter	

Various therapeutic factors are available to treat osteomyelitis, including the concentration of therapeutic drugs in the blood. The concentration of the drug requires that the concentration is at the maximum in the serum in order to give its pharmacological effect in the peripheral site [43]. This high concentration in the serum has side effects that are not reassuring for doctors and thus cause a narrow therapeutic window for patients with osteoarthritis, and therefore requires the development of new systems for drug delivery and away from the concentration of drugs [44]. The field of controlled drug delivery has gone through several stages since the beginning of the 1950s; three generations of drug delivery systems were developed. The first generation of drug delivery systems mainly includes the release mechanism such as solubility control, diffusion control, ion exchange control in oral and dermal drug delivery [45, 46]. The second generation is also called intelligent drug delivery systems on the zero system's release, for example, nanoparticles, polymers, and hydrogels to deliver proteins and peptides [47, 48]. The third generation of controlled drug delivery systems includes delivery systems modified in their structure and surface. They can penetrate or overcome chemical, physical, and biological barriers [49, 50]. Drugs are one of the essential components in our lives that we cannot dispense with and in order to obtain satisfactory results for our various disease states. Due to the aging of people in the world and various diseases, the use of medicines has increased steadily, side effects have also [51]. These side effects that appear from time to time are due to one of the following reasons, such as practice error, increase or decrease in the therapeutic dose. In the previous years, several mechanisms and drug carriers have been developed, especially for the local secretion of antibiotics and proteins, to control the bacterial infection that results from implants and enhance bone growth [52]. Calcium silicate (CS) and other compounds such as silica-based mesoporous nanoparticles have been found as promising materials, which can be prepared by several methods such as sol-gel or wet methods [53]. With silanol in the CS improve the loading capacity and control the release of drugs for long periods [54]. Delivery of drug molecules to the specified site through controlled drug delivery systems is one of the ideal methods, firstly through the quality of drug use to reduce the dose in it, and secondly through not repeating the drug intake [55, 56]. Regular release rates and release intervals require careful assessment of pharmacokinetics at the site of excretion, and the

design of an optimal delivery method for drug use quality, effective dosage, and drug release kinetics requirements [57, 58]. Although nanomaterials have lately entered the research arena, more than 250 products have already been approved and have undergone different clinical trials. Their ultimate clinical applications pose significant challenges [59].

1.1.5. Synthetic Bioceramics As x-Ray Contrast Agent

X-ray imaging is one of the best diagnostic methods used frequently in the biomedical field. It is essential to distinguish between the human and artificial tissues [60]. Iodine molecules and barium sulfate suspensions were used as contrast agents [61]. A study showed that the ProRoot Mineral Trioxide Aggregate (MTA) has a radiopacity to range from 5.34 mm Al to 6.92 mm [62, 63]. Gabriela Ciobanu et al. studied the effect of incorporating 1 wt. % of bismuth into the apatite layer via the $Ca^{2+} \leftrightarrow Bi^{3+}$ substitution process. The results showed that the incorporation of bismuth improved the radio capacity of HA [64]. Bismuth aluminate at 6% and 9% is an effective alternative agent for imaging calcium phosphate cement in clinical application for bone repair [65]. The radioactivity of the new CS based cement was evaluated, and TheraCal LC, Biodentine, Dycal, and GC Fuji IX GP were compared. Barium and strontium were used as radiation filter materials, and it was found that Biodentine TM, which contains zirconium as a radioactive element, has higher radioactivity values [66].

1.2. PROBLEM STATEMENT

In orthopedic reconstructive surgery, osteomyelitis, which causes a bacterial infection, is one of the serious complications faced by the doctors. Pure or modified CS could be use as carrier for drugs and controlled its release at the surgery site. Bioactive CS could be a suitable carrier for antibiotics. However, it’s seen as radiopaque shadows on radiographic images, either due to the fillers themselves or because of secondary reactions; such findings may present a diagnostic challenge to radiologists, dentists and orthopedists.

1.3. OBJECTIVES OF THESIS

The main objective of this thesis is to create a vehicle that will be used as a carrier for different kinds of antibiotics with improving in X-ray radiographic images.
This study aims to:

- To prepare novel compositions of CS and La-doped CS nanostructure and then will be characterized using X-ray Powder Diffraction (XRD), X-ray photoelectron spectroscopy (XPS), Scanning Electron Microscopy, Brunauer-Emmet- Teller (BET), Thermogravimetric Analysis (TGA) and Fourier-transform infrared spectroscopy (FTIR) techniques.
- To explore bioimaging properties of the prepared materials using radiographic imaging (X-ray).
- To evaluate loading/release capacity of entire materials using cephalexin hydrate (CPA), gentamicin sulfate (GEN), and Ampicillin sodium (AMP) crystalline antibiotics.

1.4. SIGNIFICANT OF THESIS

Bioactive CS plays a significant role in bone tissue and filling dental defects. The project aims to produce new biomaterials. These materials are synthesized in a modest, and low-cost method, which can be manufactured locally (in Turkey), reducing the high cost and the ordinary citizen can benefit when needed in dental restoration, and is very promising in biomedical applications, especially in future in the biomedical industry.

CHAPTER 2

LITERATURE REVIEW

2.1. CALCIUM SILICATE

Ca^{2+} has important roles to play within the living body, such as the balance of fluids within cells, muscle contraction, regulates heartbeat, plays an essential role in blood clotting, works to form strong bones and teeth, and works to regulate nerve impulses, also oocyte activation. The human body needs a lot of Ca^{2+}, especially during children's growth period, during pregnancy, and breastfeeding, its deficiency leads in the future to osteoporosis, and this may lead to the risk of fractures [67]. In addition, CS is generally composed of Ca^{2+}, Si^{4+}, O_2, and sometimes hydrogen is present in its formulations. They are always found in wet form because they contain different percentages of crystallization [68]. It is a class of inorganic compounds, and it has many forms in many different shapes and chemical compounds, including dicalcium silicate (Ca_2SiO_4), tricalcium silicate (Ca_3SiO_5), and Ca_3SiO_7 [69]. Rankinite (Ca_3SiO_7) is one of the most common types of CS. Upon contact with body fluids, including saliva, it turns into a phase similar to the components of natural bones [70]. CS decomposes in body fluids different factors control its decomposition such as corrosion, chemical composition, and molecular. In addition, CS decomposes according to the aqueous medium's crystal structure, pH, and temperature [71, 72]. Various types of CS ceramics have been developed in recent years, such as wollastonite (CS), hardystonite ($Ca_2ZnSi_2O_7$), diopside ($CaMgSi_2O_6$), akermanite (Ca_2MgSiO_7), bredigite ($Ca_7MgSi_4O_{16}$), and merwinite ($CaO_3MgSi_4O_{16}$) is a very active area for normal bones and has a functional role in the growing bone and blood vessels [73]. However, CS, silicate (SiO_2), and calcium oxide (CaO) ceramics have been used extensively in biomedical applications as bone substitutes due to their osteoconductivity biocompatibility, high osteoconductivity, and their similarity to human apatite in hard tissues [74]. After Hench and Anderson discovered bio-glass

in 1969, several ceramics related to living bones followed, containing all the CaO and SiO_4 glass-ceramics [75]. In the previous years, studies were conducted in CS powder and ceramic (β- CS and α- CS) that are bioactive and can form a layer of apatite when exposed to simulated body fluids (SBF) [76, 77], and human saliva [78]. In study of Ni, Siyu et al. the results showed that the degradation rate of CS was much faster than that of β-tricalcium phosphate (β-TCP) and Mg_2SiO_4 ceramics. As apatite were formed on the CS ceramics rapidly after cultivation. However, it was very unlikely to occur on surfaces of β-TCP and Mg_2SiO_4 ceramic surfaces. The ionic products from CS and Mg_2SiO_4 extracts could stimulate the proliferation of osteoblast-like cells at a certain concentration range throughout the 6-day culture period [79]. CS is a biomaterial that allows excellent attachment and proliferation of osteoblast, thus promoting apatite formation, making it a candidate in hard tissue repair [80]. Possibility of bioactivity, controlled release behaviour, this feature made it ideal for use in orthopedic implant applications [81], also has the property of chemically integrating into the structure of living bone tissue [82]. Several previous studies indicated that Ca_3SiO_5 is a bioactive-cement, a catalyst for HA formation when immersed in SBF. It is injectable, has a slow dissolution, and has a stimulating effect on cell growth. It is compatible and bioactive, has a biodegradable property, it also has a hollow nanostructure important in drug and protein loading/release and a high specific surface area. All these excellent properties have distinguished it in many applications such as repairing bone defects, absorption of proteins, absorption of heavy metal ions, and drug delivery properties [83-87]. *In vitro* and *in vivo* studies showed the main advantage of CS. It integrated with hard tissues, I. e. , its bioactivity directly results from the formation of Si-OH on its surface when exposed to body fluids [80, 88]. Ca^{2+} and Si^{4+} ions can stimulate bone proliferation and differentiation prepared with synthetic cement of various types of stem cells, like human adipose tissue-derived stem cells (hADSCs) [89-92]. However, traditional CS based bioceramics do not have a good porosity structure, limiting their use in drug delivery [68]. Orthopedic treatment is one of the problems that doctors face, especially infections, tumours, and fetal deformities [93]. Moreover, in orthopedic reconstructive surgery, the biggest challenge is the inflammatory process, and to treat this problem by modern methods is to introduce a system that releases the drug locally at the site of transplantation. Its advantages include high delivery efficiency,

continuous-release, reduced toxicity, and is comfortable for the patient [85]. Bioactive scaffolds must be designed with multiple functions, such as stimulating cells to form new bone, blood vessels, and drug delivery. But preparing such scaffolds has become a major challenge for researchers [94]. The ordered mesoporous materials have the characteristics of having a network of channels with a specific nanoscale (2-50 nm); additionally mesoporous materials have large specific area often greater than 300 m^2g^{-1}. This property makes them strong candidates in drug delivery processes [95]. Pore size is important in loading the drug and other materials. The portion to be encapsulated and the channel diameter have to be taken into account before deciding on any porous host matrix. When the portion to be absorbed is greater than the pore fluid, the physical absorption will only occur on the outer surface of the porous material. When the target portion is shorter than the diameter of the pores, absorption will occur in both the inner portion of the pore and the outer surface of the host matrix [96, 97]. Drugs are usually simple organic groups on the nanometer scale, with sizes reach from a few to several dozen angstrom units. These drugs would not have any difficulty entering the mesoporous channels. Absorption is usually limited to the inner part of the pores and the outer surface of the matrix particles. As for the metal-based drugs that are employed in the cancer treatment to target the deoxyribonucleic acid (DNA) is more complex, such as platinum and ruthenium drugs due to their large size, due to the formation of organometallic complexes with different organic groups, these drugs find it difficult to penetrate the mesoporous [98]. Porous CS was prepared for drug delivery properties, were studied in GEN, the result was that GEN was loaded 109.33 μg/g and the volume of mesoporous was 200 nm [99]**.** Xiaoxuan Guo et al. A studied the interactions between functional groups of drug molecules and mesoporous of CS hydrate prepared using an ultrasound method. Two types of drugs were incorporated into the CS hydrate, namely, sodium alendronate and GEN sulfate. Drug loading capacities (DLCs) were measured using thermal analysis to determine the relationship between drug transporter, interactions, and drug loading capacity. Their results showed that the acidic functional groups of the drug correlate with the active sites of CS hydrate, which are Ca-OH and Si-OH through electrostatic interactions [100].

Table 2.1. Loading sensitivities of the Ca-OH and Si-OH groups to different functional groups of drug molecules.

Functional Group	**Ca-OH**	**Si-OH**
Carboxylic acid (R−COOH) groups	+	+
Phosphonic acid groups	+	+
Amino ($R-NH_3$) groups	-	-
R−OH groups	-	-
Sulfuric acid groups	+	+

"+" means that the functional groups will interact with one Ca-OH or Si - OH; "-" means that no reaction occurs.

Fan, Y., Huang, S et al. have successfully developed a europium-doped mesoporous CS (Eu^{3+}-MCS) possessing a bioactivity property. (Eu^{3+}-MCS) was performed as a carrier for ibuprofen (IBU) delivery. The luminescence observed when showing europium under Ultraviolet (UV) irradiation, the intensity of europium emission of Eu^{3+} varies in the IBU carrier system according to the amount of IBU released. Thus the drug release process can be easily tracked and monitored by changing the brightness intensity in the drug delivery process [92, 101]. In another study, a Eu^{3+}/Tb^{3+} doped MCS was prepared. Their results showed little cytotoxicity, as well as drug storage/release properties in mesoporous for IBU. Mesoporous obtained can be used to store and release medicines. IBU was used as an example in loading drugs. Under the influence of UV irradiation, samples loaded with IBU showed characteristic emission lines for both Eu^{3+} and Tb^{3+}. The luminescence intensity of Eu^{3+} in the drug carrier system increased with increasing the cumulative amount emitted from IBU, and this made the drug trackable and monitored by changing the luminosity of Eu^{3+} [102].

2.2. DOPING OF CALCIUM SILICATE

The creation of new advanced materials with high properties can improve the strength, size and morphological structure. However, significant fundamental changes are not possible in the properties and behaviour of materials unless the properties of the material are changed at the molecular and nanoscale level and this depends on the methods see table (2.2). In addition, the various nanoforms may act as nucleating agents for the formation of CS hydrate.

Table 2.2. Summary of technique for preparation CS shape and positive and negative points.

Method	Dopants	Morphology	Notes	Refers
Sol-gel	Eu-CS	At 800°C the particles are homogeneous and well distinguished, spherical shapes. Thick 7 mm and diameter 2-3 nm.	When the temperature increases, the thickness and diameter decrease. After doping improve hierarchically porous. When the amount is large, it may be cytotoxic.	[103]
	La-CS/Chitosan	Crystal uniform distributed, has 3D macrospores, size of ~200 μm.	The granule diameter improves with increasing heat. Sizes are big and amorphous	[104]
	hybrid chitosan/CS	The particles were dense in the form of white balls with well spread surfaces. The size of 20-53 nm.	Improved in mechanical proprieties. Some of the reaction products may remain as OH group.	[105]
	Sr-CS	A bean-like shape, grain size under 200 nm.	Improve morphological proprieties. Affected in the structure, and in the porosity network.	[106]
	Mg-CS	Has a smooth surface with regular and lumpy spherical shapes. The size decreases when increasing amounts of	Improve the bioactivity. High cost for fabrication.	[107]

		Mg.		
Precipitation	CS	Nano-spherical morphology, 20-100 nm.	It has a short cycle. The added reagents are not strong enough to break all bonds.	[108]
	CS	3D hierarchical networks, more uniform blocks, size is ~ 1-2 nm.	Reducing the number of reaction steps. Adjustment of pH may be necessary.	[109]
	Cu-CS	15 nm long needle shapes lumpy irregular, size is 12-36 nm.	Improved in Mechanical proprieties. Produces high concentration after added precipitate.	[110]
Hydrothermal	CS	Long fibers in leafy forms, Size 10-20 nm.	Manufacture of high-quality large crystals. High cost of equipment.	[111]
	CS	A sponge-like shape of spherical, Size 2-6 μm, also 15-40 nm.	The cost is low compared to other methods. Their products are not of good purity.	[112]
	La-CS	Ball-like particles with sizes from 230-510 nm.	Improve morphological proprieties. Big amount is cytotoxic.	[113]

2.3. LANTHANUM AND LANTHANUM DOPED CALCIUM SILICATE

La^{3+} is a suitable host for a good number of bioceramics. Especially with the excellent luminescent property of the following colors red, green and blue due to its excellent thermal and chemical stability. Emission appears from the visible region to the near infrared region [114]. Rare earth elements (REEs) such as La^{3+}, cerium (Ce), and ytterbium (Yb) are found in healthy bones and their aggregation contents change with age [115]. REEs are characterized by higher density, greater thermal conductivity, as well as a high melting point [116], and they have peculiar physical and chemical properties so they have been widely applied in biomedical applications [117, 118]. Moreover, its oxides play an effective role in improving the strength of the bio-composites during the sintering stages. This feature makes them suitable for biomedical applications. It is a rare metal with properties of utmost importance in biomedical applications. It is antibacterial, has good mechanical strength [119], and has the property of bone resorption inhibition [119]. La^{3+} plays an essential role in the manufacture of radiation shielding glass [120]. Previous studies showed, Lanthanum oxide (La_2O_3) nanoparticles were prepared and found the anti-bacterial activity of these particles was evaluated, showing inhibitory effects against Gram-positive bacteria on *Staphylococcus aureus*. Additionally, nanoparticles were made of La^{3+} and Ca that showed clear effects on *Pseudomonas aeruginosa* [121, 122]. However, La^{3+} is one of the elements that can replace the Ca^{2+} element in HA in human bone; this substitution has an effective role in overcoming the biological and mechanical [104] and physicochemical properties of HA [123]. It was found that when La^{3+} is added to apatite, it improves some physicochemical properties, such as thermal stability, higher bending strength, better biocompatibility and less toxicity [124]. HA doped lanthanum and loaded with amoxicillin. The results showed that La^{3+} led to a delay in releasing amoxicillin [124]. In addition, studies have shown the properties of lanthanum-silicate (La-Si) co-substituted apatite. The incorporation of these ions elements into the apatite structure increased the biocompatibility of the coating. It was found not to cause toxic effects of mesenchymal stem cells [125]. It can regulate vital bone mineralization as well as metabolism and it can accelerate the bone resorption [104]. The La^{3+} ion must be controlled in the body within the safe concentration range, but the mechanism of bone formation for biomaterials based on

La^{3+} is not yet known [126]. There are studies conducted between pure La_2O_3 and HA, but there are still no reports on HA and La_2O_3 toxicity. However, high concentrations of pure La_2O_3 should be avoided [127]. Studies in recent years have shown that compounds that based on La_2O_3 in their composition tend to deposit in bone tissue. Clinically, the food and drug administration (FDA) has approved lanthanum carbonate under the name (Fosrenol®) for the treatment of hyperphosphatemia in patients with kidney failure and dialysis [128], but it was utilized as phosphate binders [123]. However, recent studies have noted that long-term treatment with lanthanum carbonate can improve bone abnormalities in these patients. Results confirmed in animals for postmenopausal osteoporosis reported that lanthanum carbonate can also improve bone formation that appears through an increased trabecular density [129]. M. I. Ahymah Joshy et al. showed that the La-HA was improved certain properties such as higher flexural strength, lower dissolution rate, excellent biocompatibility, and higher thermal property compared to pure HA. In addition, their results also indicated that adding La_2O_3 to HA prolonged the release of the drug, and it has antimicrobial properties against both gram-positive and gram-negative bacteria [130]. Gautam et al. prepared pure HA nanopowder by microwave irradiation, and lanthanum hydroxide was added. HA and La_2O_3 composites were synthesized in different concentrations of 0.1, 0.2, 0.3 and 0.5 wt. % by conventional solid-state pathway. The aim of this method is to enhance the mechanical properties. Their results were that the highest concentration of La_2O_3 was at 0.5wt. % by weight showed good mechanical properties, such as density, compressive strength and load-bearing capacity. Its density was higher than the normal bone density, at a rate of 2.85 g/cm^3, on the contrary, the normal bone density of 2.2 g/cm^3. It also obtained the highest compressive strength of 108.89 MPa, its fracture hardness reached 130.06 mega joules/cm^3, Young's modulus of 90.75 GPa, and both compounds had a porosity enabling them to be used in the fields of biomedical engineering. HA and 0.5% of La_2O_3 are certain in terms of mechanical properties very close to normal bones, and are biocompatible for bone tissue engineering applications [131]. Xiao-Yuan Peng and his colleagues attended a three-dimensional (3D) porous calcium-chitosan silicate scaffold doped with La_2O_3 using a freeze-drying method. After adding La_2O_3, they were found inside the lanthanum-doped mesoporous CS/chitosan (La-MCS/CTS) scaffold on large 3D pores whose

walls contain large pores. These structures are biocompatible, promoted the adhesion, proliferation, acceleration of new bone tissue growth. Significantly, their experiments showed that La^{3+} ions in these scaffolds supported osteoblastic differentiation in rats by activating the transforming growth factor (TGF) signal pathway [104]. Furthermore, a nanoparticle of HA doped La was prepared, and La^{3+} = 0.02, 0.06, 0.1 was prepared by sol-gel method at a low temperature of 100 °C. The results showed that the greater the amount of La_2O_3, the greater the size of the crystallization [132]. Emad El-Meliegy et al. La^{3+} doped phosphate glasses nanoparticles prepared phosphate nanoparticles doped with La^{3+} at a concentration of 0.5 and 10 mol% using the modified sol-gel alkoxide technique. It aims to regenerate the bones and drug delivery applications. Their results showed that the specific surface area and pore size significantly decreased after adding La to it. For the modified La, a faster ionic release was observed than the phosphate glasses in water and Tris-HCl. As a drug carrier, the results showed that La glasses modified could deliver ciprofloxacin over a period of 28 days compared to the standard glass. However, it was found that when the non-doped La^{3+} phosphate glasses were observed, there was early release of ciprofloxacin, and this is considered a drawback for the phosphate glasses in the delivery of ciprofloxacin [133]. CS has recently found great interest as a new class of candidates for the treatment of bone defects. Although CS has remained the mainstream of ceramic bone substitutes, their clinical use is limited due to suboptimal mechanical properties. The table 2.3 shows the type and quantity of the dopants, preparation method, and the effect of the dopants on CS.

Table 2.3. Showing CS Doped with Different Dopants and Their Aims.

Composition	Dopants	Method	Notes	Refers
$Ca_2SiAl_2O_7$	1, 2, 5 and 10 % strontium (Sr^{2+}).	solid-state sintering method	Have *in vitro* osteogenic properties for bone regeneration.	[134]
CS	10 mol% strontium (Sr^{2+}).	Precipitate method	The regeneration of osteoporotic bone defects.	[135]
CS	5% of strontium and zinc ions	Sol-gel method	The incorporation of Sr and Zn into CS scaffolds has a notable role in the stimulation and differentiation and proliferation of mouse bone osteoblasts *in vivo* and *in vitro*.	[136]
Ca_2SiO_4	0.04g Mg^{2+} ions	a classical Strober method and a template based solve-thermal process	After doping magnesium to Ca_2SiO4, the surface area of CS increased from 185.68 $m^2g^{-1}$to 212.71 m^2g^{-1}. This resulted in a more than 50% increase in the loading capacity of the anticancer drug doxorubicin.	[137]
CS	0, 2.5, 5, 10 and 20 mol% of Eu^{3+}.	Coprecipitation method	The incorporation of europium ions to reduce the crystal size, achieve photoluminescence and the intensity increases as the amount of europium increases.	[138]
CS	1, 2, 5 mol of Eu^{3+} ions.	Facile hydrothermal synthesis method	The addition of europium ions made the matrix emit red luminescence, making the matrix a promising candidate for bioimaging. The matrix also has a large pore size that makes the matrix highly efficient in drug loading, sustainable drug release as well as pH	[139]

			responsive.	
CS	0, 2, 5 and 10 % Sr^{2+}.	Triblock copolymer (P1 23)	The incorporation of Sr and with an increase in the amount of Sr was observed to stimulate osteoblasts, control the rate of drug release to some extent, and also have the potential to regenerate bone tissue.	[140]
CS	1, 3, 5, 7 and 10% CuO^{2+} ions	Wet precipitation method.	CS was doped with copper and doxycycline was loaded, the release rate was about 71.43 to 96.38, and this depends on the amount of the cupper.	[141]
CS	0.41, 0.82 mol for Mg^{2+} And 0.20 , 40 for Mn^{2+}	Sol-gel	CS co-doped Mg; Mn, scaffold has been shown to be effective in forming new bone *in vitro* and in vivo, as well as in forming vascularization. The difference between the Mg and Mn scaffold in chemical, physical and biological properties.	[142]
CS	0.15-0.3 mol LaB6 ions	Facile route of Sonochemical method.	After doping La^{3+} borate to CS, the matrix had a specific surface area and large pore size. These two agents make up the matrix for the release of IBU, up to about 312h at SBF.	[143]
CS	0, 10, 20% La^{3+} ions	Solid-state method.	CS was prepared pure and doped in varying proportions. The compound is considered as an alternative candidate for cell culture.	[113]
CS	2.5, 5 % Sr^{2+} ions	Sol-gel method	It plays a major role in enhancing bioactivity, and due to its large pore size after doping, it can be a good proposal for controlled drug delivery applications.	[144]

CHAPTER 3

METHODOLOGIES

3.1. MATERIALS AND METHODS

Calcium nitrate tetrahydrate (Ca $(NO_3)_2 \cdot 4H_2O$, Merck-Germany), Sodium metasilicate (Na_2SiO_3, Merck-Germany), and Lanthanum nitrate hexahydrate (La $(NO_3)_3 \cdot 6\ H_2O$, Sigma-Aldrich Ltd) were used to prepare pure CS and La-doped CS materials. Gentamicin sulfate ($C_{19}H_{40}N_4O_{10}S$, Sigma-Aldrich Ltd), Cephalexin hydrate ($C_{16}H_{17}N_3O_4S \cdot xH_2O$, Sigma-Aldrich Ltd), and Ampicillin sodium ($C_{16}H_{18}N_3O_4S.Na \cdot H_2O$, Sigma-Aldrich Ltd) antibiotics were used as drug model to evaluate loading and release behavior of CS and La doped CS materials.

3.2. PREPARATION OF CLCIUM SILICATE AND LANTHANUM DOPED - CALCIUM SILICATE MATERIALS

The CS and La-CS materials were prepared using the wet precipitation method. An 11.81g of Ca $(NO_3)_2 \cdot 4H_2O$ powder dissolved into 100 mL of distilled water. A 6 g of Na_2SiO_3 powder dissolved into 100 mL of distilled water at lab temperature. Then, $Na_2SiO_3 \cdot 9H_2O$ solution was added dropwise to Ca $(NO_3)_2 \cdot 4H_2O$ under stirring till obtaining white precipitate. The white precipitate solution was kept under stirring for 12 h. The white precipitate was collected and washed several times to neutralize the pH value and remove nitrate (NO_3) ions. Then, the white precipitate was dried at 80℃ overnight, then grounded and calcined at 900℃ for 2 h. The La-CS materials were prepared using the same protocol. About 5%, 10%, and 20% of La $(NO_3)_3 \cdot 6\ H_2O$ was added to the Ca $(NO_3)_2 \cdot 4H_2O$ solution. The amount of chemicals used to prepare pure CS and La-CS materials were summarized in Table 3.2.

Table 3.1. Molar quantities of reactants used for the synthesis of CS and La-CS.

Sample ID	**Reactants**						
	$Ca(NO_3)_2 \cdot 4H_2O$		Na_2SiO_3		$La(NO_3)_3 \cdot 6\ H_2O$		La (wt %)
	mol	gr	mol	gr	mol	gr	---
CS	0.5	11.81	0.5	6.11	0.00	0.00	0%
1La-CS	0.475	11.22	0.5	6.11	0.025	1.01	5%
2 La-CS	0.425	10.04	0.5	6.11	0.05	2.17	10%
3La-CS	0.325	07.67	0.5	6.11	0.1	4.33	20%

3.3. CHARACTERIZATIONS

3.3.1. X-Ray Diffraction

The phase purity of the prepared materials was investigated using X-ray diffraction (XRD, Rigaku MiniFlex Desktop XRD. Japan). The samples were scanned from 20º to 80º in 2θ angle, and the lattice parameters were calculated using the integrated software package. The phase purity of the entire materials was detected via matching with standard patterns (Joint Committee on Powder Diffraction and Standards (JCPDS)).

The average crystallite sizes of the synthesized samples were calculated using the Debye Scherrer formula Eq (3.1):

$$D = k\lambda/\beta\cos\theta \qquad (3.1)$$

Where D = average crystallite size, λ: is the wavelength of X-rays used β: is FWHM (full width half maximum) is the X-ray diffraction line, θ: is the diffraction angle, K: is a constant equal to 0.68 to 2.08, and 0.94 for spherical crystallites with cubic symmetry). For crystallite size calculations, we used the FWHM at (0 0 4), (1 1 3), (0 2 2), (1 1 4), (-2 0 4), (-2 2 1), (3 0 0), (-1 3 1), (3 1 1), (0 4 0) and (-2 2 7) reflections.

The crystallinity of the synthesized samples for CS and La-CS was calculated using this formula Eq (3.2):

$$\text{Crystallinity} = (Ac/Am)*100 \quad (3.2)$$

Where Ac: Area of all the crystalline peaks, Am: Area of all crystalline peaks and amorphous.

3.3.2. Fourier Transform Infrared Spectroscopy

Fourier transform infrared spectroscopy (FTIR) is used to identify the functional groups. FTIR technology is of great interest to researchers and has important advantages such as speed, accuracy, and relative sensitivity. In this technique, the samples are subjected to contact with infrared (IR) rays. The infrared rays affect the atomic vibrations of a part in the sample, leading to absorption or specific energy transfer. The FTIR technique is thus very useful in determining the specific molecular vibrations present in the sample. FTIR spectra were acquired using FTIR instrument (FTIR, Bruker IFS 66/S, FRA 106/S**,** Germany**)**. The collected data for all samples in the range of 400 to 4000 cm^{-1}

3.3.3. X-ray Electron Spectroscopy

X-ray electron spectroscopy (XPS) is an advanced surface analysis technique used to obtain chemical information about the surfaces of solid materials. This device works by scattering photoelectrons using a beam of X-rays whose main objective is to excite atoms on the surfaces of solid materials. The spectrum provides information about the chemical environment and oxidation state of the element. Separate chemical states with close energies are separated using peak detection software, giving each state's content as a percentage. In this technique, an (XPS, PHI 5000 Versa Probe) spectrometer was used on an argon ion gun that allows depth analysis on the sample's surface and substrates. The X-ray beam can focus from 10 µm to 200 µm.

3.3.4. Scanning Electron Microscopy

Scanning electron microscopy (SEM) is one of the most important methods for studying surface formation by scanning it with a high-energy beam of electrons. These electrons interact with the atoms of the compound, producing surface topography images, and this technique, a SEM (QUANTA 400F Field Emission. USA) was used. This device produces high-resolution images of the sample surface to understand the surface structure. For this method to work, samples must be electrically conductive on the surface before examining the sample with an electron microscope. The samples for both CS and La-CS were coated with a very thin layer of gold-palladium alloy for electrical conductivity. The mean particle size and particle size distribution were determined by measuring mean sizes. SEM images were randomly selected, using analysis software ImageJ (National Institutes of Health, USA) for image analysis.

3.3.5. Thermogravimetric Analysis

Thermogravimetric analysis (TGA) is a technique used to determine the thermal stability and a fraction of volatile components. It monitors the weight change when the sample is heated at a constant rate. In this technique a Thermal Balancer or Thermal Weight Analyzer (TGA, Instruments SDT 650 Simultane DSC/TGA) was used, and all materials were heated at a temperature of 20 - 1200°C. Using an asynchronous differential scanning meter and a thermogravimetric analyzer, the weight change and heat flow of materials are simultaneously measured as a function of temperature or time. Thus, the thermal stability of the material and moisture determines the proportions of volatile components or additives.

3.3.6. *In vitro* Loading and Release of Antibiotics

3.3.6.1. Discs Shaping

The as-synthesized powders were compacted by uniaxial cold press to a disc shape (12 mm in diameter and 1 mm in thickness) using an automatic hydraulic machine [Carver] at 5000 lbs. load, then sintered at 900°C for 2h.

3.3.6.2. Preparation of Stock solution and Calibration Standards

The stock solution of AMP, GEN sulfate, and CPA hydrate antibiotics were prepared to evaluate the loading and release capacity of CS and La – Cs materials. About 300 mg of each antibiotic dissolved in 300 ml of distilled water.

Various dilutions for each antibiotic were prepared. About 10%, 20%, 40%, 60%, 80% and 100% of the stock solution were synthesized. Part I: The λ_{max} was found to be at 280 nm for AMP and GEN, and 290 nm for CPA, using Ultraviolet-visible spectroscopy (Biotek 25 UV/Vis Spectrophotometer, USA). The calibration curve was constructed by plotting the concentration versus absorbance. Part II: As in method 1, the absorbance of each sample was calculated based on λ_{max}. Part III: Third, the transmittances for each sample were calculated by the following formula Eq (3.3):

$$Y = mx + b \tag{3.3}$$

Where Y is the absorbance, Y: molar absorptivity (L/mol.cm), x: Concentration (mol/L), b: in the first equation Path length = 1cm λ_{max} (nm).

3.3.6.3. Drug Loading and Release Test

The samples (in the disc shape) were immersed in 20 mL of antibiotic solution (100mg/100mL) and stored 24, 48, and 72h at lab temperature. At each interval point, 1 mL is taken from the antibiotic solution (later substituted by 1 mL fresh distilled water) and measured absorbance. The antibiotic concentrations were

determined from a previously plotted calibration curve with known concentrations of antibiotic solutions.

The release profile of antibiotics from the pure CS and La- CS discs were carried out using distilled water for 24, 48, and 72h at lab temperature. The discs were immersed in 20 mL of distilled water. Every 24h 1 mL of drug solution was taken and 1 mL of distilled water was added. The absorbance was calculated for all samples as in the drug loading method. The experiments were performed in triplicate.

3.4. X-RAY CONTRAST IMAGING MEASUREMENTS

The Radiopacity of pure CS and La-CS materials (in the disc shape) was investigated. A meaty tissue was used from the hind legs of a sheep. Medium holes the size ~12mm was made. A one-way x-ray film was taken.

3.5. STATISTICAL ANALYSIS

All quantitative assessments were taken in triplicate (n = 4), and results are expressed as mean ± standard deviation (SD). Statistical comparison of data for different compositions was carried out via a two-way analysis of variance (Graph Pad 8) using the Origin 8.5 programs from Origin Lab. Differences were considered statistically significant at $p < 0.001$.

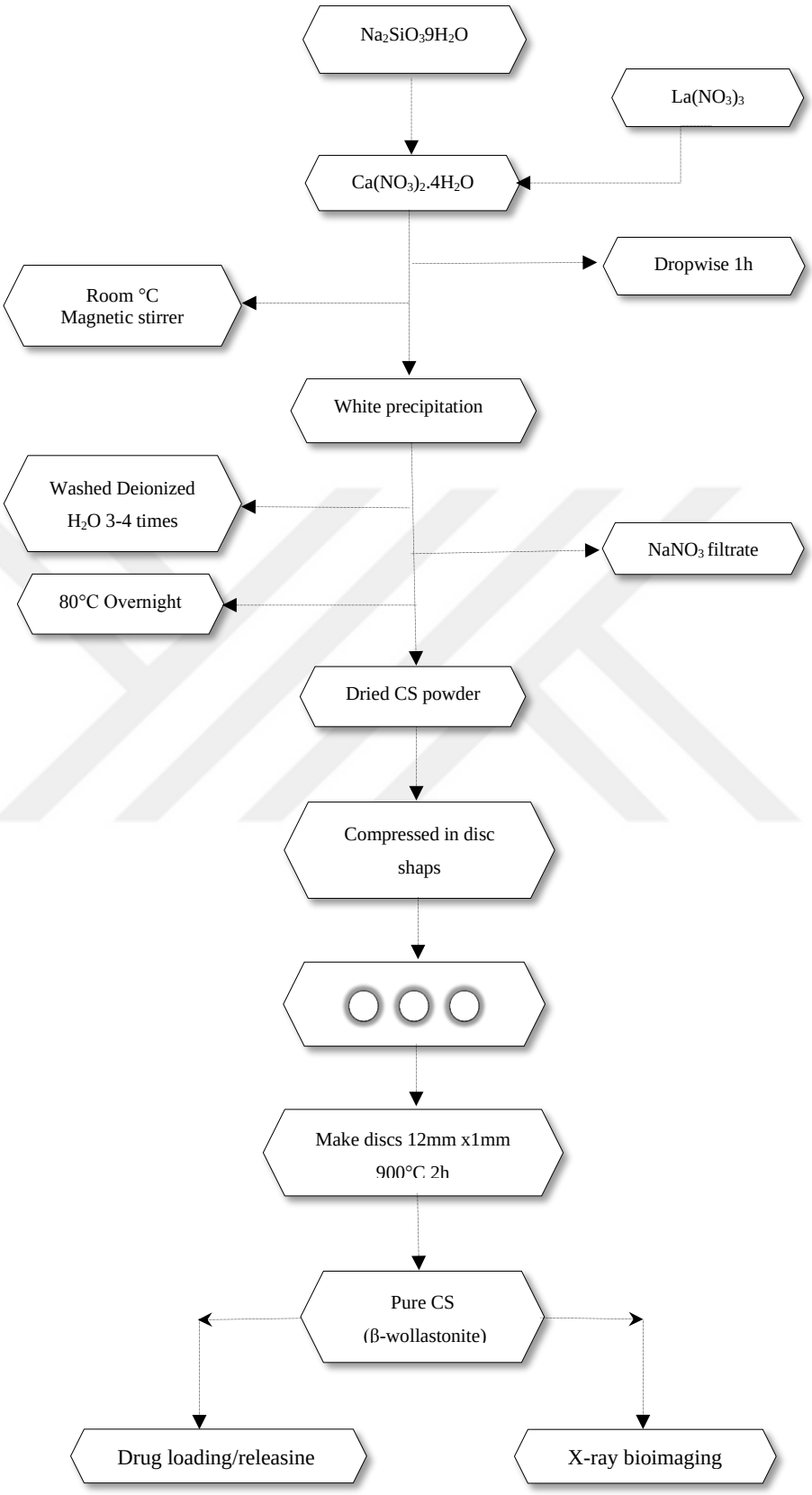

Fig: 3.1. Flowchart of Thesis

CHAPTER 4

RESULT AND DISCUSSION

4.1. PHYSICOCHEMICAL CHARACTERIZATIONS

4.1.1. X-Ray Diffraction

XRD patterns of pure CS and La^{3+} doped CS calcined at 900°C for 2h were illustrated in Figure 4.1.

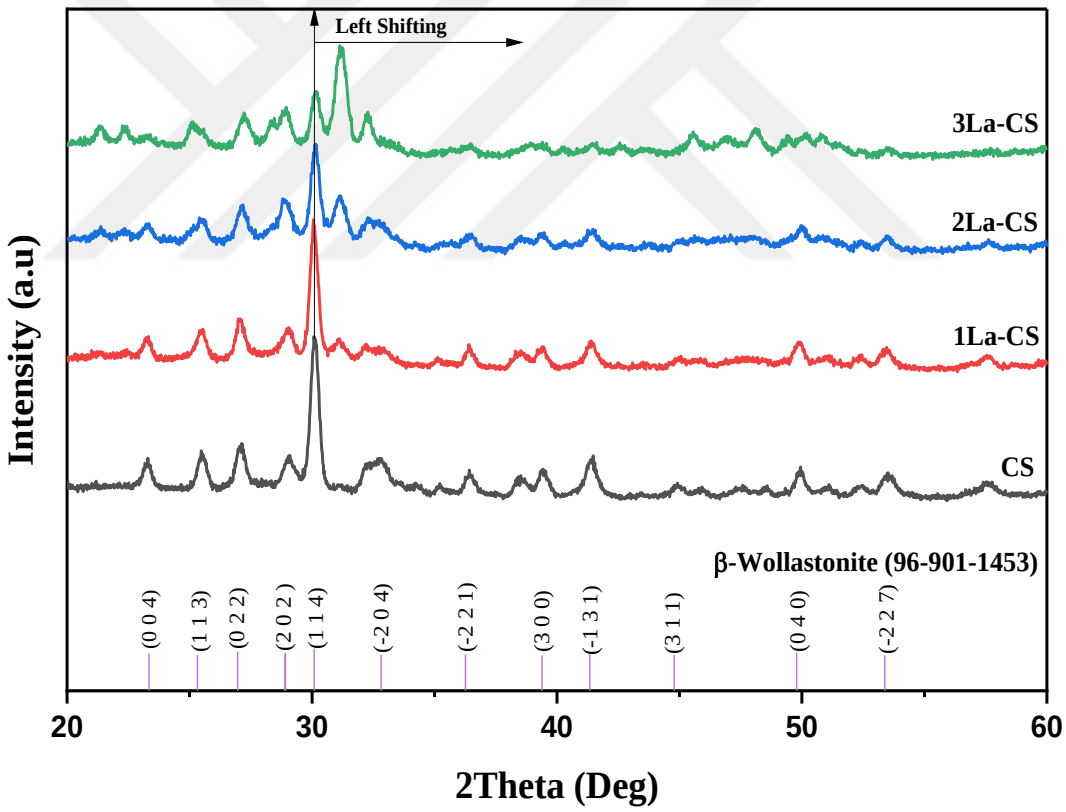

Figure 4.1. XRD patterns of CS and La-CS materials were calcined at 900°C for 2h.

The XRD result for pure CS show a crystal structure with prominent diffraction peaks, at 23.3°, 25.5°, 27.1°, 30.1°, 36.0°, 41.1°, and 49.4°, which is consistent with that standard phase of Wollastonite (Fig. 4.1) [145]. Other phases haven't been detected, which confirmed the phase purity of CS. The diffraction peaks that appeared in sharp and narrow shapes revealed that the synthesized CS shows a reasonable degree of crystallinity. The average crystallite size of the CS crystals was 106 nm. The obtained results were in good match with Adams, Luqman A et al. [146]. With the incorporation of La^{3+} ions into CS crystals, the intensity of diffraction peaks of CS was decreased, the width was expanded, and the locations of peaks were shifted to the high value of 2 thetas. These influences could be attributed to the substitution small ionic radius of Ca^{2+} ions (0.099 nm) with a higher ionic radius of La^{3+} ions (0.116 nm) with a small ionic radius of 0.099 nm. The addition of La^{3+} led to a decrease in the lattice parameters, crystallite size, and degree of crystallinity of CS crystals (Table 4.1). However, the fluctuation in the crystallite size could be assigned to lattice strain which can distort the crystal lattice of the CS structure [147]. Hence, these metal ionic exchanges can lead to minimal distortion of bonds in the crystal structure of CS [148].

Table 4.1. The lattice parameters, degree of crystallinity, and crystallite size of pure CS and La-CS materials.

Samples ID	**Lattice Parameters**				**DC (%)**	**CrS (nm)**	**PS (nm)**
	a (Å)	**b (Å)**	**c (Å)**	**V (Å)3**			
JCDPS (β-Wollastonite)	15.4231	7.3220	7.0630	789.163	-----	-----	----
CS	15.4210	7.3183	7.0407	763.965	82.6	56.1	106
1 La-CS	15.4175	7.3159	7.0386	757.423	73.2	50.6	120
2 La-CS	15.4141	7.3011	7.0348	742.430	66.6	51.3	203
3 La-CS	15.4240	7.2985	7.0301	738.873	60.8	42.4	198

Where is the DC (%), CrS (nm), and PS (nm) represented the degree of crystallinity, crystallite size, and particle size, respectively.

4.1.2. Fourier Transform Infrared

The functional groups of CS and La-CS materials were evaluated using FTIR, and the obtained results were displayed in Figure 4.2. The bending modes of Si–O–Si were located at 682, 883, and 932 cm^{-1} which matches the study reported by Sreekanth and colleagues and Saravanan et al. [149, 150]. The bending mode of the Si–O band was detected at 420 cm^{-1} and 644 cm^{-1} which assigned due to the vibration of Si-O bonds in silicate tetrahedra. The absorption bands occur at 1010 and 1060 cm^{-1} because of the Si–O vibration and are similar to those described by Adams, Luqman A and Ismail, Hamisah et al [146, 151, 152, 153]. Furthermore, the vibration bands at about 1072 and 500 cm^{-1} are attributed to Si-O-Si asymmetric stretching and Si-O-Si bending respectively [154]. Incorporation of La^{3+} ions had a remarkable effect on the FTIR spectrum. With an increasing amount of La^{3+} ions gradually shifted the band of Si-O-Si at 450-867 cm^{-1} to 449-904 cm^{-1}, along with expansion in the peak area. The broadening of the peak was attributed to the reduction in the crystallinity which was also observed in XRD analysis (Table.4.1). However, it can see that the band broadness at 712–981 cm^{-1} slightly increased for La-CS when compared with pure CS. After doping, it is noticed that the band intensities become weaker with respect to the increase of La^{3+} content from 5 to 20 wt% in CS. This broadness of bands and weaker intensities indicate the minor structural changes in CS by the inclusion of La^{3+} [155]. The pure and La-CS exhibit the characteristic functional bands at 450-867 cm^{-1} to 449-904 cm^{-1}, 712-981 cm^{-1}, and 1016–1078 cm^{-1} which corresponded to the bending mode of Si-O-Si, symmetrical stretching band of O–Si–O, Si-O-Ca bonds containing non-bridging oxygen and asymmetrical stretching mode of Si-O-Si group, respectively [156, 157]-[155]. Besides the expected peaks, a carbon peak at 1394 or 1635 cm^{-1} was detected due to the carbonate ion (CO_3^{2-}) in the aragonite phase [158, 159]. These carbon impurities have atomic ratios ranging from 22.1 to 29% for different samples. This peak does not affect the interpretation of our results and, in fact, was actually used to calibrate the bending energy by setting the bending energy to 284 eV to correct for the sample charging [160]. Maybe the source of this carbon contamination was most likely due to the adventitious deposition of hydrocarbon contaminants from the atmosphere [161, 162]

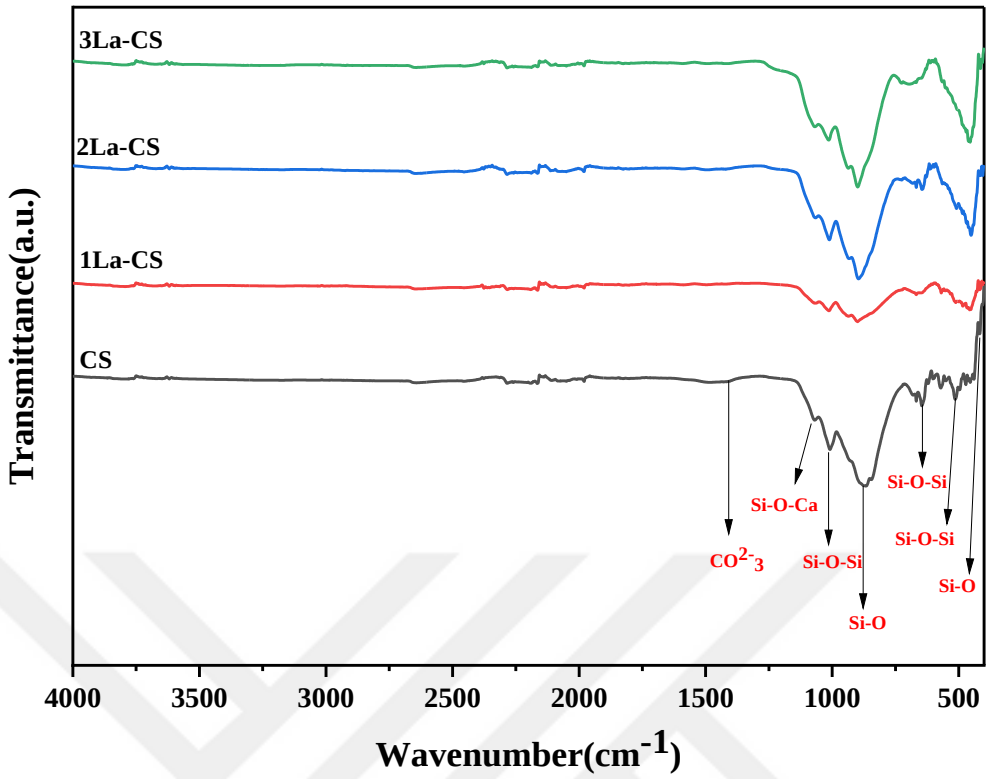

Figure 4.2. FTIR spectra of CS and La-CS materials calcined at 900°C for 2h.

4.1.3. X-ray Photoelectron Spectroscopy

XPS technology is a useful tool for the quantitative determination of surface components and sample compositions. XPS was used to investigate the chemical compositions of CS and La-CS and the results were displayed in Figure 4.3. The XPS spectrum indicates that the existence of La^{3+} in the CS crystal lattice and represented in the range of binding energy from 0 to 1100 eV. It can see that the Ca(2p), Ca(2s), Si(2p), Si(2s) Si(2s) and O1s elements with the binding energy of 345, 436, 101-102, 152, 24 and 530 eV respectively were observed [163]. Thus, the main components of CS and La-CS were O, Si, Ca, and La, indicating that pure phase of materials was obtained [164, 165]. The binding energy of Si (2p) was observed in the range of 102 to 101 eV. These binding energies are similar to those reported for CS cement [166]. There was a slight decrease in the binding energies of Si (2p) with increasing Ca/Si, indicating

that silicate depolymerization [167], as observed for crystalline silicates. In all spectra, peak narrowing was observed with increasing Ca/Si, indicating increased structural ordering [168]. After incorporation the La^{3+} with CS, new binding energies appeared at 1La-CS, 2La-CS and 3La-CS showing the presence La^{3+}. It was found that the presence of La (3d), Ca (2p), Si (2p), and O (1s) elements with the same binding energies, as for the binding energy for La, it was 831-852 eV. The binding energy of valence state La (3d) was divided into two groups of peaks such as 3d5 and 3d3. In this spectrum (1La-CS, 2La-CS, 3La-CS), significant peaks were observed at a binding energy of 831, 833 and 831eV which were assigned to La(d), and peaks around at 851, 852, 855 eV corresponded to 3d5/2 respectively. The peak at 833 eV was an overlap between La3d5 and La3d because the La3d3 (835 eV), La3d (853 eV) lines were closely located. It can be seen that the relative amount of La^{3+} present at the surface of these powders increased gradually. For La-CS at the point 834 eV, it confirms the incorporation of La^{3+} ions into CS structure; whereas detection of La^{3+} ion at this location was considered as La in La-CS which was confirmed by previous studies [160, 169]. In the Table 4.3 the theoretical part, the ratios of La/Ca and (Ca+ La)/Si ratio differ according to the quantity of the materials. In the practical part, using XPS Ca-binding energies are relatively independent of CS composition or structure, and as the La/Ca ratio increases, the (Ca+ La)/Si ratio increases. However, at low La/Ca ratios, the binding energies are slightly higher, as a result of both the slightly shorter Ca-O bonds between the silicate anions and the Ca^{2+} and the decreased Ca^{2+} coordination in these compounds. This results in increased screening and relaxation of Si^{4+} atoms, leading to lower binding energies. The trends in Si^{4+} photoelectron binding energies may also be understood in terms of the (La+Ca)/Si ratio of the silicate anions [170].

Table 4.2. Show La/Ca and (Ca+ La)/Si ratio using XPS.

Sample ID	Theory		Practical Using XPS	
	La/Ca	(Ca+ La)/Si	La/Ca	(Ca+ La)/Si
CS	0	1.440	0.0084	0
1La-CS	0.107	1.514	0.0652	0.4623
2La-CS	0.255	1.536	0.0882	0.4868
3La-CS	0.668	1.558	0.2323	0.5313

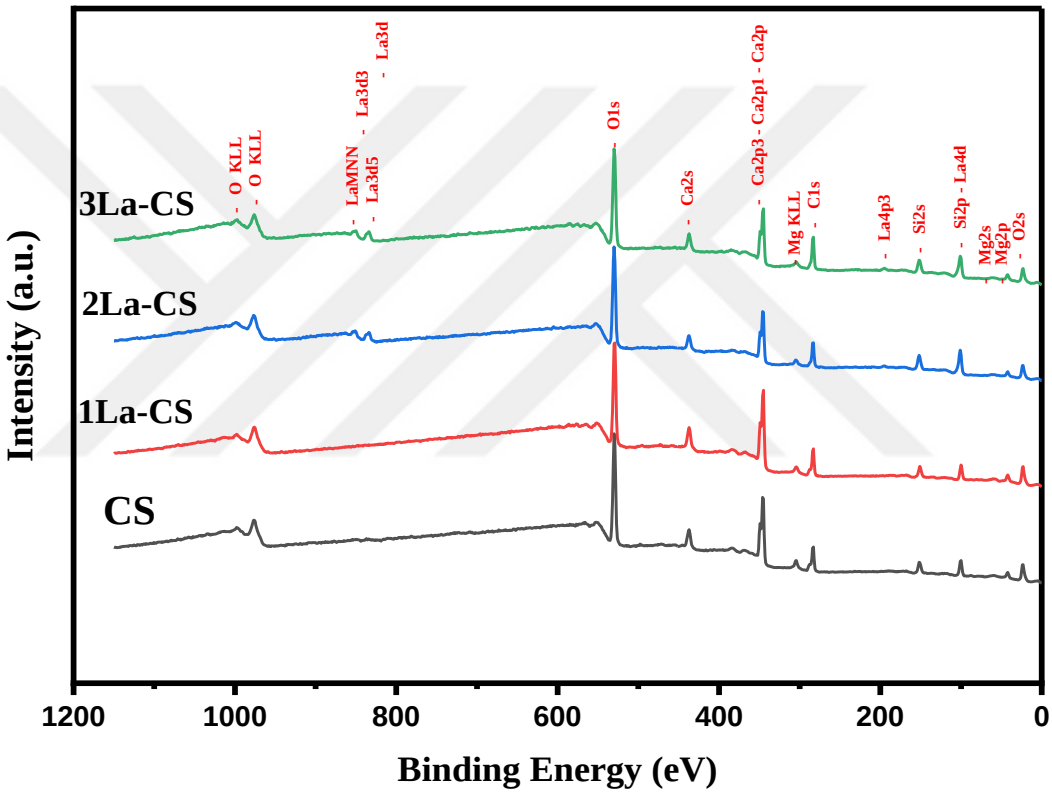

Figure 4.3. XPS patterns of CS and La-CS nanocrystals sintered at 900°C for 2h.

4.1.4. Scanning Electron Microscopy

Figure (4.4) show the SEM micrographs of CS and La-CS, the CS particle appeared in heterogeneous microstructure composed of crystallites of different sizes and irregularities of shapes. It is clear that powders have quite distinct properties in morphology. The results showed also that the micrographs of pure CS are densely packed and in multiple layers, this explains that the incorporation of La^{3+} ions did not have a noticeable effect on the shape morphology of CS. The growth rate of CS particles was found, and, it is diminished by the increasing amount of La^{3+} ions content in the composites, this study agreed with the study of Jadalannagari et al [132, 171, 172]. However, the average particle size estimated from the SEM micrographs was observed higher than the size determined by the Scherer equation (Table 4.1b in XRD). The mismatch between the SEM micrographs and the Scherer equation is attributed to particle fusion and leads to particle agglomeration. This study matches a study by Motameni, Ali et al. on the La^{3+} doped tricalcium phosphate βTCP [171].

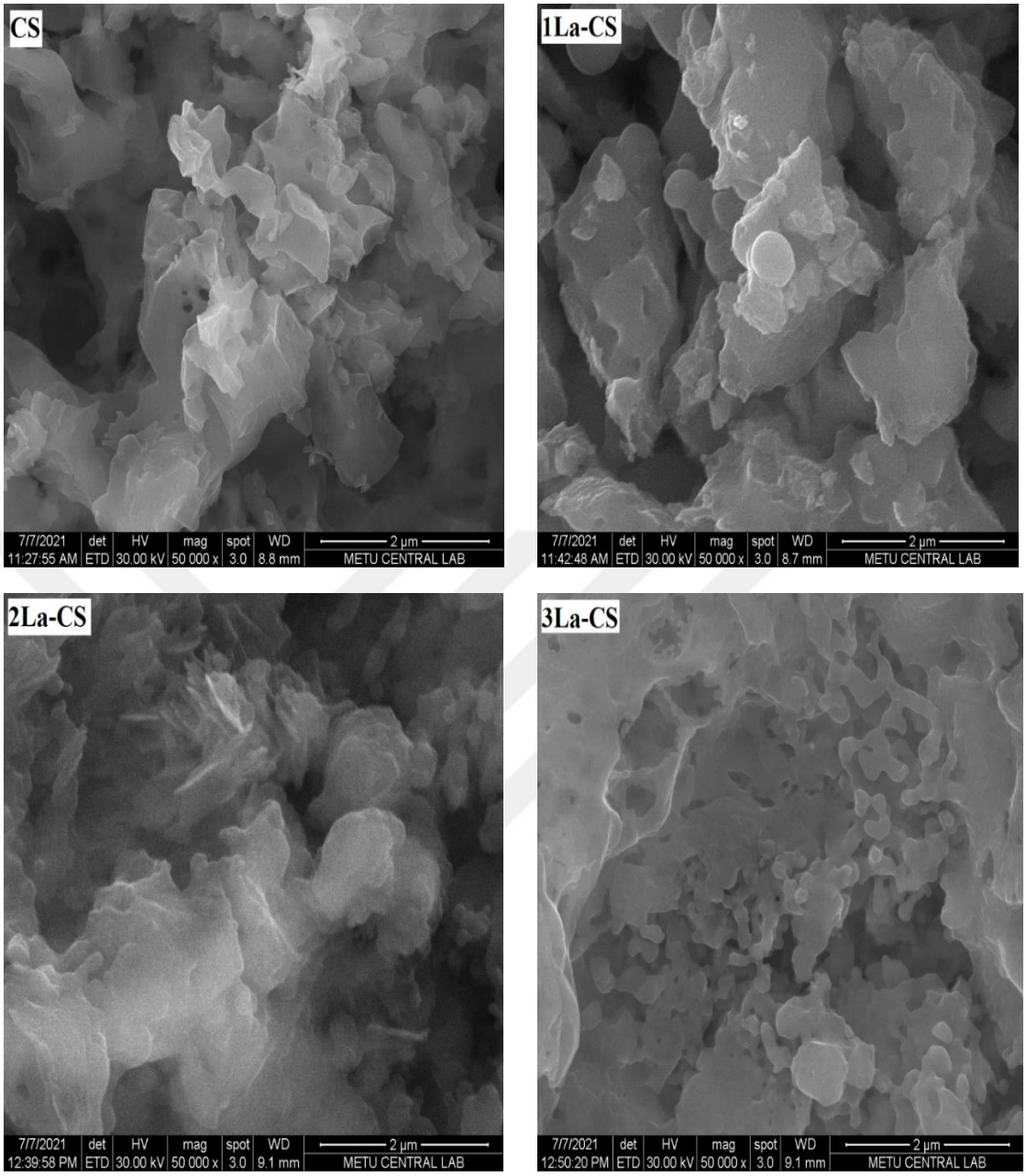

Figure 4.4. SEM patterns of CS and La-CS nanocrystals sintered at 900°C for 2h.

4.1.5. Brunauer-Emmett-Teller

The structural properties (specific surface area, volume, and pore size) of CS and La-CS were studied using the N_2 adsorption-desorption isothermal method. According to the international union of pure and applied chemistry (IUPAC) classification, the type IV isotherms for all prepared materials are accompanied by the narrow hemispherical meniscus, capillary condensation [173], which confirmed that the

obtained material have mesoporous . The four sample materials were characterized for their average surface area and pore size distribution evaluation. The synthesized nanoparticle revealed a large surface area with variable pore size depending upon their different concentrations of La^{3+} doping. The synthesized CS exhibits the highest surface area of 9.742 m^2g^{-1} with a pore size distribution of 3.503 nm The summary of the BET isotherm represented in Table 4.5, which is in good match with the previous reports on the preparation of silica-based materials [174]. After the inclusion of La^{3+} fluctuating in the values of surface area, pore volume and pore size was observed (Table 4.5). The average surface area is 7.074 m^2g^{-1} (pore size 3.917 nm) and 5.496 m^2 g^{-1} (pore size 2.250 nm) for 2La-CS and 1La-CS respectively. For the 3La-CS the average surface area is 3.378 m^2 g^{-1} (pore size 2.129 nm), Weiya Huang et al. When the actual La^{3+} adding gradually increase from 4.19% to 22.44%, the specific surface areas of the Lanthanum-doped ordered mesoporous with zero La^{3+} decline from 987.48 m^2 g^{-1} (Lanthanum-doped ordered mesoporous hollow silica spheres-1/50) to 420.38 m^2g^{-1} (1/5 lanthanum [175]. However, the pore volume and specific surface area of CS decreased after adding a large amount of La, and the pore size increased [176]. The amount of N_2 adsorbed increased, when the amount of La increased, this indicates that there is a noticeable change after the addition of La, which leads to shrinkage in the size of the pores (Table 4.5). In addition, fluctuations and differences in the value of the surface area, pore-volume, pore size, shape, and size were observed in the samples, which may be due to the incorporation of La ions into the CS [176, 177].

Table 4.3. Specific surface area and average particle size of CS and La-CS

Sample ID	**S. Surface Area (m^2/g)**	**Pore Volume (cm^3/g)**	**Pore Size (nm)**
CS	9.742	0.0244	3.503
1La-CS	5.496	0.0963	2.250
2La-CS	7.074	0.0108	3.917
3La-CS	3.378	0.0071	2.129

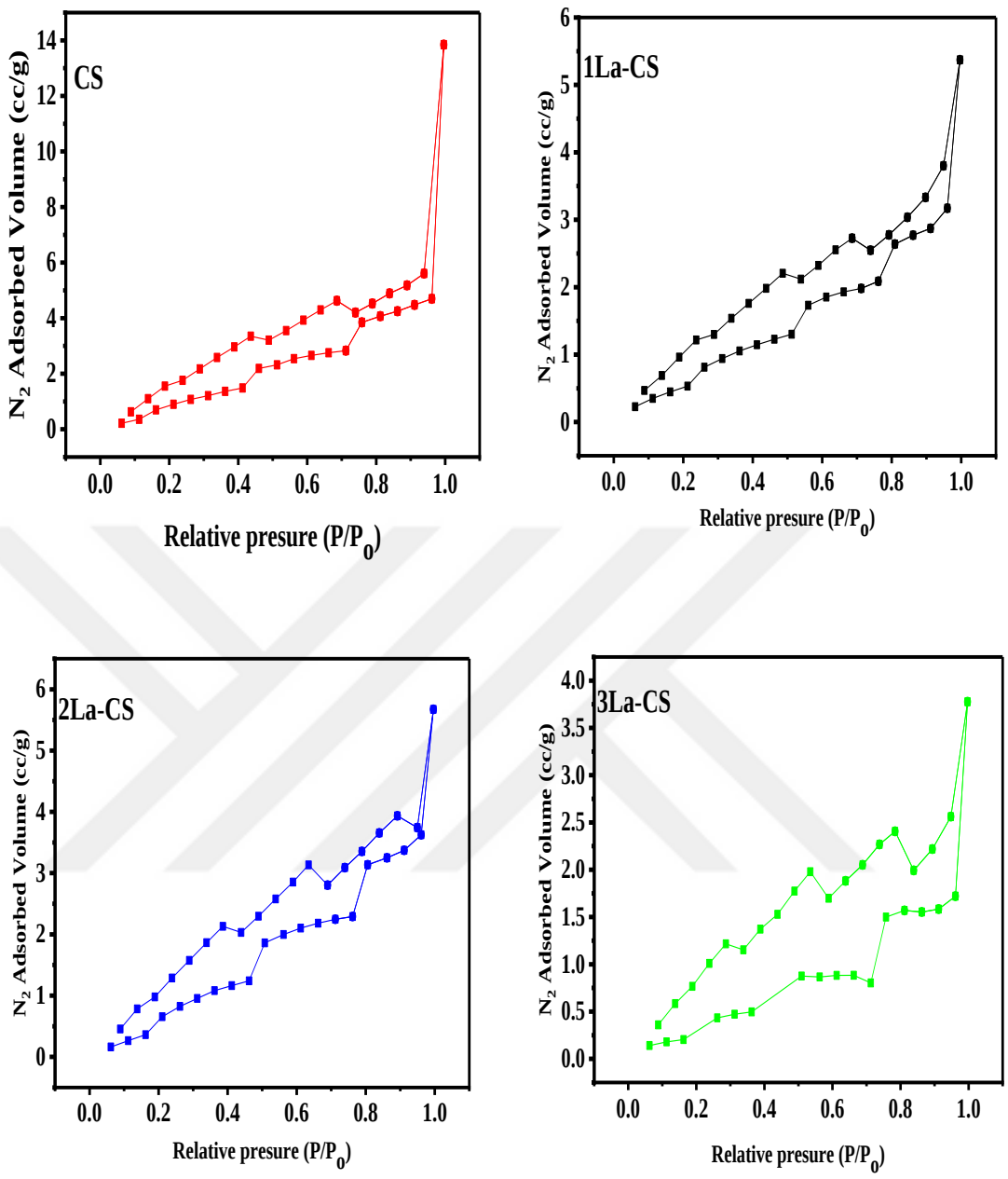

Figure 4.5. N_2 adsorption-desorption isotherm.

4.1.6. Thermogravimetric Analysis

In Figure 4.6 shows the TGA curves for CS and La-CS powder calcined at 1200 ºC. For all the samples the weight loss was clearly observed in three stages: 20-220 ºC: this range corresponds to the loss of adsorbed water molecules from the surface of the samples, and also the condensation of the silanol groups present on the surface of the nanoparticle samples. For 1La-CS, there was a loss of approximately 11% by weight, while 2La-CS recorded a significant weight loss of about 42% by weight in the same range, mainly due to its ability to absorb more water molecules. Zakaria Tabia et al. studied TGA magnesium doped Bioglasses the first range between 30 °C and 220 °C corresponds to the loss of physically adsorbed water molecules (from 30 to 120 °C) and they also observed condensation of silanol groups (from 120 to 120 °C) [151]. Bilgin et al. was also observed when studying calcium phosphate cement at 30°C - 250°C, the removal of lattice water [178]. In the range of 220-650°C: an average weight loss was observed for all samples, about 5-9% by weight, which could be due to the disposal of residual nitrate and carbonate groups that did not react during synthesis and the decomposition of left-out organic groups in the precursor. Kushal Singh et al. in TGA the step from 250 to 600 °C can be related due to decomposition of nitrates (major) and carbonates (minor) present in the sample [179]. R. Lakshmi et al. studied wollastonite in the range 280-600 °C The loss in this range is due to the decomposition of left-out organic groups [159]. In the range 650-760ºC and above: weight loss reached steady state for all samples (2-10 wt %). After adding La (NO_3), a high percentage of weight loss was observed, especially in La-CS, reaching 50.55%. This can be explained by the fact that La (NO_3), as dopants, delayed the loss of part of the water did not completely decompose at low temperatures; its decomposition was at temperatures higher than the normal temperatures. Some of the organic matter left over at a temperature of over 650 °C is removed. Nobuaki Yamaguchi et al. From the results of thermal analysis of dicalcium silicate, the burning temperature was set at 650 °C because the weight loss from the decomposition of calcium nitrate $CaNO_3$ it will be completed 850 °C [180]. Javier Peña-Poza et al. studıed TGA lanthanum-Silica, the weight loss was higher in samples doped with La (NO_3) due to the lack of release of adsorbed water in addition to lanthanum salts. The highest weight loss percentage of La $(NO_3)_3$ doped sample

could be explained by the early decomposition of nitrate groups at about 60 °C, which cannot be discarded [181].

Table 4.4. Weight loss of the CS and different La-CS dopants according to the temperature.

Sample ID	Temperature Range (°C)	Weight Loss (%)	Total Loss (%)
CS	32-197	9.25	25.86
	197-623	5.87	
	623-728	10.74	
1La-CS	40-237	10.92	26.02
	237-632	6.10	
	632-726	9.63	
2La-CS	27-108	42.23	50.55
	108-644	6.13	
	644-746	2.19	
3La-CS	29-101	28.49	44.40
	101-651	9.80	
	651-718	6.11	

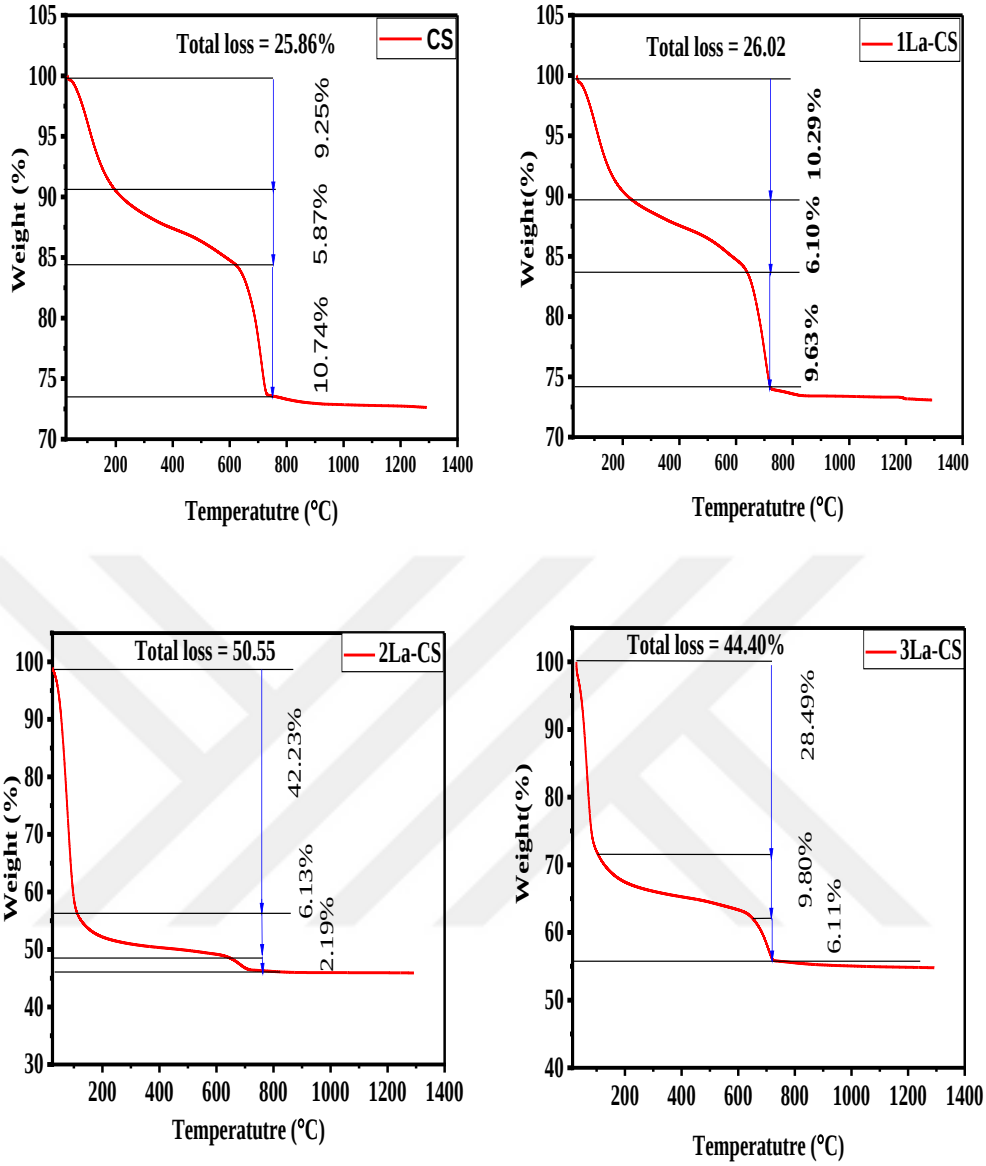

Figure 4.6. Thermograms of CS and La-CS composites calcined in the range 20-1200°C.

4.2. X-RAY CONTRAST IMAGING MEASUREMENTS

The radiopacity of CS and La-CS were determined and shown in Figure 4.7, for the pure CS radiopacity showed an ambiguous luminosity, and this luminosity was caused by a low intrinsic radiopacity came from CS. This was confirmed by previous studies of Camilleri, J. Et al. That CS exhibited a low intrinsic radiopacity value of 1.62±0.29 mm Al [182]. After doping by La^{3+} which has atomic number (Z) = 57, the results showed that there is a difference in the luminosity of the variance; which varies according to the amount of La^{3+} added show in figure 4.7. There is a significant which contrast observed for the disc, 2, 3, and 4, show the differences between the different discs, this is in agreement with the previous study of Watts [183]. A high radiopacity strength study after doping Portland cement with zirconium oxide showed radiopacity above the minimum recommended by ISO/American dental association (ADA) of 3.0 mm Al which is 4.19±0.31 [184]. The Z of material plays a crucial role in radiopacity [185]. The element with a higher Z has more inner shell electrons that block more photons, resulting in a high radiopacity value [186]. In the study of Chiehfeng Chen, MD et al. CS was doped with zirconium (Zr) oxide (Z = 40), barium (Ba) sulfate (Z = 56), tantalum (Ta) oxide (Z = 73) and bismuth oxide (Z = 83) were used as radiopacifier materials. The results revealed that the radiopacity generally increased when the Z of the radiopacity clear was higher. However, the radiopacity of CS/Zr was higher than that of CS/Ba, although the Z of Zr was lower than that of Ba [187]. In addition, a recent study by Camilleri and Gandolfi, their study showed that cement based on CS which has (Z = 20) after adding zinc oxide which has (Z = 30) to it gave sufficient radioactivity by 30%, demonstrating the importance of a high Z to obtain adequate radiopacity [182]. In another for Marco Antonio Hu´ngaro Duarte et al. study that obtained a similar result, zirconium oxide was used as a radiopacifying agent for CS, showed that the radiopacity did not reach the limit of 3.0 mm of Al scale required by ISO 6876; it specifies the characteristics and measurements of radiopacity. When tested the sealer and in accordance with the standards, it must have a radiation capacity of at least 3 mm of Al. but it improved the image became progressively more radiopaque [188]. On the contrary, Aguilar, Fabiano Gamero conducted a study in which they used bismuth with a concentration of 20%, which has

a higher (Z = 83), and zirconium oxide, which has a lower (Z = 40), according to the results obtained in this study. That all cements will behave in a similar way this behaviour could be attributed to several parameters such as quantity, receptor type, exposure time [189, 190]. Chen, Chiehfeng et al. the radiopacity depends also depends on the arrangement or density of the atom [187]. This study has unified all the variables and has defined the optical density is a logarithmic measure of the ratio transmission incident light through the film image and depends not only on the X-ray absorption properties of the materials but also on the characteristics of the film and the exposure and processing conditions [183].

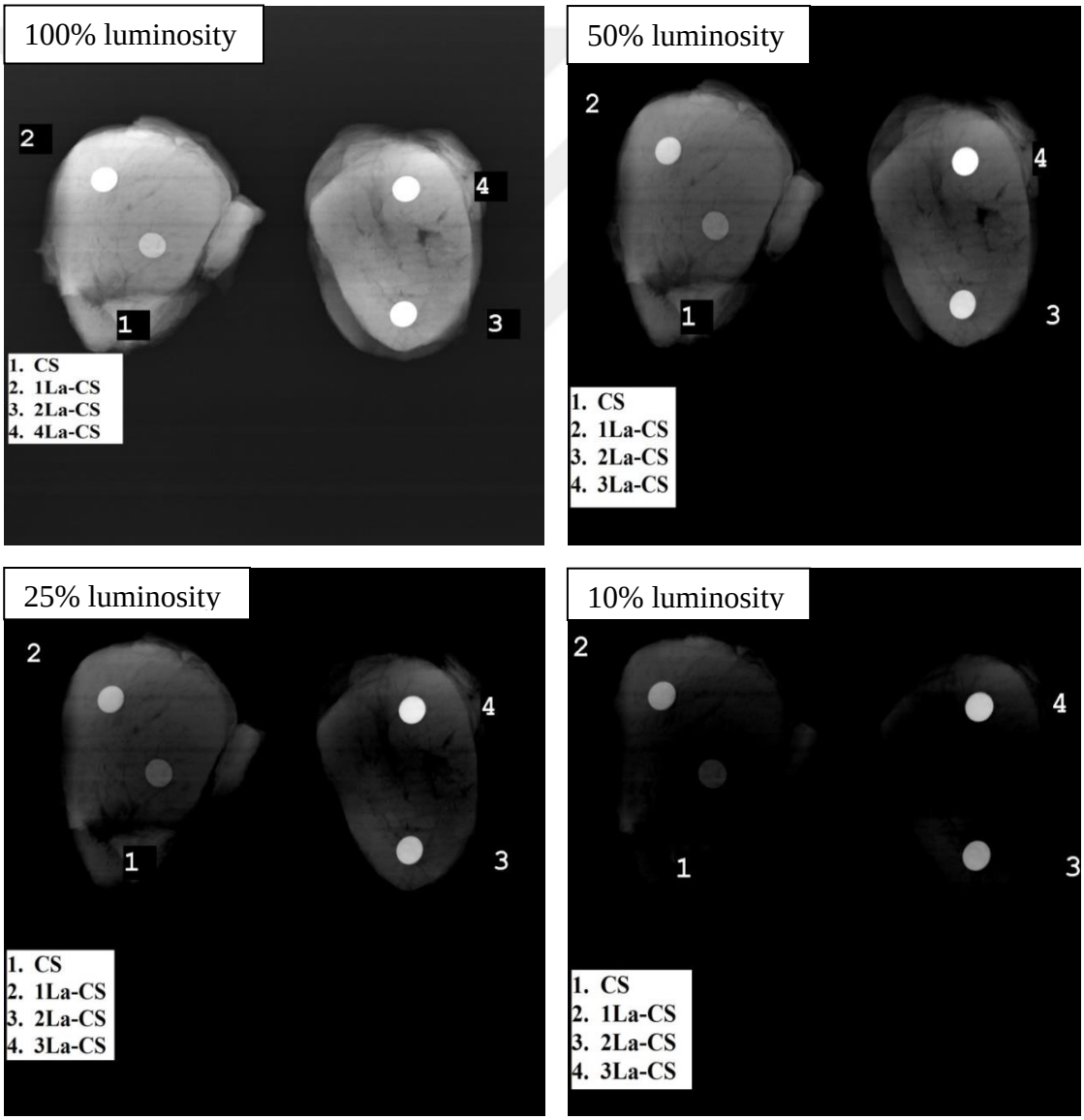

Figure 4.7. Bioimaging patterns of CS and La-CS nanocrystals with different doping conditions.

4.3. DRUG LOADING AND RELEASE MEASUREMENTS

The drug loading behavior of both CS and La-CS was investigated. AMP, GEN, and CPA were used as models to evaluate the loading and release capacity of CS and La-CS materials. Figure 4.9 shows the loading capacity of antibiotics on the surface of particles for 24, 48, and 72 h. The maximum loading rate of antibiotics was on the first day of incubation, the loading rate gradually decreased with a prolonged incubation period, whereas the minimum loading rate was reported on the third day of incubation. This behaviour was expected, the amount of drugs decreased in the stock solution due to the increasing dilution rate. In pure CS the drug loading was 1.1530 mg of AMP was loaded during the first 24 h which was the highest loading for pure CS, followed by 0.5852 mg of CPA and 0.1996 mg of GEN. At 48 and 72 hours, the highest CS loading was for AMP. This loading efficiency depends on the interaction of the drug substances via hydrogen bonding, and this is explained by the formation of hydrogen bonds between functional groups such as the hydroxyl group in CS and the carboxyl group in drugs, which in turn accelerates or slows down the effect of loading the drug at once; this was pointed out by Yong Fan et al [191]. The rapid loading of the drug at the beginning of the loading time resulted from the physical absorption of the europium-doped CS of IBU on the surface of the compound or near the entrances to the channels. As for the slow loading or the sustained loading, it is due to the bonding of the drug with the hydrogen bonding compounds. These hydrogen bonds are stronger than physical adsorption [101]. In addition, in a similar study, CS cement was also prepared and it was loaded with bisphosphonate risedronate, an anti-osteoporosis drug. They also showed in their experiments that the loading process can last for six months, and an initial explosion was also observed in the first two days, after which the loading was slow and continuous. The loading increased by 1% starting from the third for 5 the months [192]. Chengtie Wu et al. CS nanoparticles have the ability to load drugs with high capacities such as AMP, reaching up to 20.69 mg/g. A sustained loading process of two weeks was detected, and the accumulative loading of AMP is about 30%, which shows an excellent property of drug delivery through CS mesoporous [193]. Hang, C., et al. prepared mesoporous La hexaboride doped CS was prepared as a drug carrier; the results showed that the surface area of the compound LaB_6 doped CS is

higher than LaB_6, this feature made the compound distinguished in drug loading. Use the drug IBU for loading; the loading rates were more than 65%, which is much higher than the loading of the drug on CS mesoporous [143]. In another study, cerium-doped HA was prepared and the loading capacity of the drug was about 43%, compared to Pure-HA, the study used IBU as drug loading. This is due to its pore size ~ 0.152 cm^3mg^{-1}, and the average pore diameter of 7-8 nm. The first loading was rapidly, followed by a controlled drug loading [194]. With the addition of La^{3+} ions, the loading capacity was increased and the highest loading was for 3La-CS of is reaching up to 1.2016 mg in AMP, 0.4791 mg in CPA, and 0.2238 mg in GEN. For CPA, the highest loading percentage was recorded at CS. This decreasing/increasing the loading capacity could be attributed to the narrow surface area, when a proportion of lanthanum was added to CS, the surface area decreased from 9.742 to 3.378 m^2g^{-1}. When a molecule is loaded and its diameter is much smaller than the pore diameter, most of the drug molecules will not be retained within the pore as part of it is loaded and the rest will not be retained. In this case, the main factor controlling the amount of trapped particles will be the specific surface area. Francisco balas et al. studied different pore diameters, 3 and 9 nm, and different surface areas, 1157 and 719 m^2g^{-1}. Both nanoparticles were loaded with alendronate under the same conditions; the maximum amount of drug-loaded was 14% and 8%, respectively. These results showed the dependence of drug loading on a surface area [195]. In addition, this can also be explained by the fact that the amide group that is present in all the antibiotics used has a role in accelerating and slowing loading factors. For AMP and CPA, which contain fewer amide groups, the rate of loading was higher, unlike GEN, which contains more amide groups. In the physical interaction between drug and mesoporous Manzano, Miguel Vallet-Regí et al. reported the stronger amide bond between the drug and the : Mobil Composition of Matter Nº. 41 (MCM-41) results in slower and more controlled loading of IBU [196]. The protonated NH_2 groups of Doxorubicin (DOX) can increase hydrophilicity at lower pH within the cancer cells, which subsequently weakens the hydrophobicity between the Graphene Quantum Dots (GQDs) surface and the DOX, inducing the loading of DOX molecules from the surface of the carrier, Yang, Xiaoying et al. [191].

In vitro drug release, many carrier systems have been used for controlled delivery. There are factors that can affect the accelerating and slowing down releasing factor. Such as molecules that are loaded on the outer surface of the carrier through a non-covalent reaction and others, hydrophobicity/hydrophilicity, and PH. The maximum drug was released in CS and La-CS at the 24h start, is given in (Fig. 4.9); the drug release profile from the CS is 0.9141 mg for AMP, 0.4968 mg for CPA, and 0.1354 mg for GEN.

With the incorporation of La^{3+} into CS, the drug release percentage was decreased. The highest release ratio was to AMP, reaching 1.0502 mg, followed by CPA 0.3875 mg and GEN with 0.1547 mg. The quantities of drugs released decrease with an increase in La^{3+} concentration. There is a sudden outburst of drugs in the initial 24h and then the drug is released in a controlled manner. The drug is released gradually over a period of time. This shows that the drug is released in a controlled manner. Such a release profile observed could provide rapid delivery of the drug, this rapid delivery gives antibacterial effects at the infected site and a sustained release to aid long-term healing and avoid the toxic and adverse systemic effects caused by a high concentration of antibiotics. Liu, W et al. was prepared Ca_3SiO_5 cement and loaded it with GEN, their results showed that the initial release was rapid, and they explained that loading the drug outside the surface is one of the reasons for the rapid initial release, after which the release stabilized. For the molecules loaded on the outer surface of the carrier through non-covalent interaction, due to this weak affinity, drug release can be easily achieved by a simple adsorption process, mostly associated with changing the state of the solvent or PH [197]. The slow release of all used antibiotics is due to the presence of the trapped carboxylic group, which reacts with Ca in the CS and La-CS. For example, the silanol groups of silica can form a hydrogen bond with its hydrophilic property [198]. These hydrogen bonds are easily interacted with by polar molecules such as water, resulting in a rapid and non-specific release. In the hydrogen bonds, Vallet-Regí et al. reported using the mesoporous silica for drug delivery, and IBU loaded mesoporous was soaked in the SBF for release. It was observed that the release was very fast in the early stage, which may be caused by the weak interaction of the acid group present in IBU with the silanol groups present on the surface of the pore wall [197]. This initial rapid release is consistent with a study by releasing GEN under conditions of 37°C and the

mean pH was pH = 1 and pH = 4. The release process showed a rapid initial release during the first three days, followed by a relatively slow release. As the concentration of GEN increased, the loading ratio was increased. The release process took place in distilled water and in PBS for more than 10 days especially with lower pH values [199]. Baker studied the effect of the slow release of ciprofloxacin in HA and zinc-doped HA, the results clarified that the reason is due to the presence of the carboxylic group in ciprofloxacin, which reacts with the calcium in HA and zinc-doped HA [200]. The release of drugs from CS nanoparticles exhibits a typical two-stage release mechanism. The drug release is high during the initial time and then it reduces and becomes constant. The drugs released during the initial burst stage are due to desorption of drug molecules that are located on the surface of the particles. These particles do not strongly interact with the CS [201].

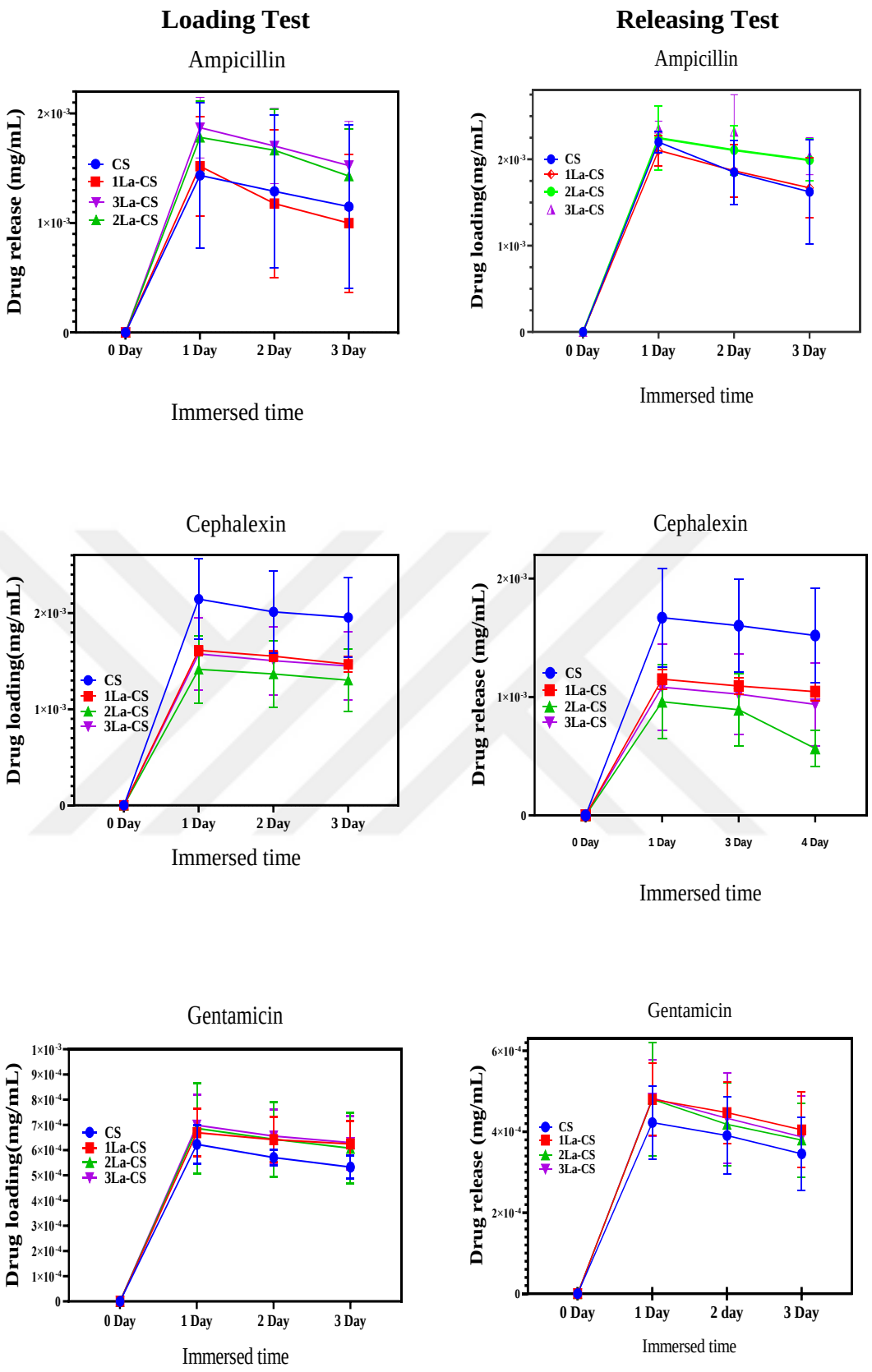

Figure 4.8. The loading and release amount of ampicillin gentamicin and cephalexin from CS and La-CS immersed in water distilled for 3 day.

CHAPTER 5

CONCLUSION AND FUTURE PERSPECTIVES

5.1. CONCLUSION

Novel multifunctional biomaterial was developed from the CS that can be used for X-ray radiographic imaging and drug delivery systems. Pure CS and La (0.5, 10, and 20 wt. %) doped CS were successfully prepared using the wet precipitation method. After incorporation of La^{3+}, some physical and chemical properties of (CS) were improved. In the XRD result the intensity of the diffraction peaks of the CS was reduced, the width was expanded, and the locations of the peaks shifted to the high value of 2θ. The incorporation of La^{3+} ions had a remarkable effect on the FTIR spectrum. With an increasing amount of La^{3+} ions gradually increased the broading of Si-O-Si band. The micrographs images show that incorporation of La^{3+} ions had no noticeable effect on the particles of CS shape. The growth rate of CS particles was diminished by the increasing amount of La^{3+} ions content in the composites. In TGA especially after incorporation of La^{3+} the percentage of weight loss of La-CS was increased. The results of CS and La-CS showed a high specific surface area of 9.742 $m^2\ g^{-1}$ for the CS sample, thus it is the highest surface area of all samples, for non-doped La-CS to 3.378 m^2g^{-1}. In contrast, La-CS the pore size is 3.3917 nm for the 2La-CS. The radiographic images of CS were significantly enhanced with the addition of La^{3+} ions. The loading capacity of antibiotics on CS particles' surface for a one-day incubation period was about 1.1530 mg, 0.5852 mg, and 0. 1996 mg for AMP, CPA, and GEN, respectively. The loading capacity significantly improved with the incorporation of La^{3+} ions into CS materials. Thus, the loading process of AMP in non-doped CS was higher than the rest of the samples due to the increase in the surface area in non-doped CS. As for the loading of AMP, the reason may be due to the lack of amide groups in the drug, as the amide group in all the antibiotics used

had a role in accelerating and slowing down the loading and releasing factor. The silanol groups also have a crucial role in the formation of hydrogen bonds with the drug and its hydrophilic/hydrophobic properties. These bonds have a rapid interaction with polar molecules, and this can affect the processes of loading and releasing.

5.2. FUTURE PERSPECTIVES

It is desirable to develop new multifunctional nano-intelligent material with multiple properties. In this regard, we suggest further investigation to verify the properties of La-CS *in vitro / in vivo* analysis to confirm the presence or not of cytotoxicity at the concentration used in this study. It can also be used as an antimicrobial drug delivery (target gene).

REFERENCES

1. Mohamed, A.M., "An overview of bone cells and their regulating factors of differentiation". ***The Malaysian journal of Medical sciences***: MJMS, 15(1): p. 4.(2008).

2. Iyer, K.M., "Anatomy of Bone, Fracture, and Fracture Healin"g, ***in General Principles of Orthopedics and Trauma.***, p. 1-17. (2019).

3. Chindamo, G., et al., "Bone Diseases: Current Approach and Future Perspectives in Drug Delivery Systems for Bone Targeted Therapeutics. ***Nanomaterials*** (Basel). 10(5). (2020).

4. Cheng, H., "Development of nanomaterials for bone-targeted drug delivery". ***Drug Discov Today***. 22(9): p. 1336-1350. (2017).

5. Chindamo, G., "Bone Diseases: Current Approach and Future Perspectives in Drug Delivery Systems for Bone Targeted Therapeutics" ***Nanomaterials (Basel)***. 10(5).(2020).

6. Soundrapandian, C., B. Sa, and S. Datta, "Organic–inorganic composites for bone drug delivery". ***Aaps Pharmscitech***,. 10(4): p. 1158-1171, (2009).

7. Iyer, K.M. and W.S. Khan, "General principles of orthopedics and trauma**".**, ***Springer*****.** p**.** 1-17 (2013).

8. Alvarez-Urena, P., 6.1 "Bioactive Ceramics and Bioactive Ceramic Composite Based Scaffolds", ***in Comprehensive Biomaterials*** II. p. 1-19. (2017).

9. Hasan, A., "Advances in osteobiologic materials for bone substitutes". ***Journal of Tissue Engineering and Regenerative Medicine***,. 12(6): p. 1448-1468. (2018).

10. Black, J.D. and B.J. Tadros, "Bone structure: from cortical to calcium". ***Orthopaedics and Trauma***, 34: p.113-119. (2020).

11. Palmer, L.C., "Biomimetic systems for hydroxyapatite mineralization inspired by bone and enamel", ***Chemical reviews,***. 108(11): p. 4754-4783, (2008).

12. Morgan, E.F., G.L. Barnes, and T.A. Einhorn, "The bone organ system": **in** ***Osteoporosis***,. p. 3-20 (2013).

13. Luo, J., "Calcium Phosphate Based Biomaterials for Bone Augmentation"., ***Acta Universitatis Upsaliensis.,*** p.55 (2018).

14. Guo, X.E., Y.J. Hu, and A.T. Dinescu, "Bone Structure and Function", ***Tomsk polytechnic university***., p.185. (2020).

16. Setiawati, R., P.J.O. Rahardjo, and b. "regeneration, Bone development and growth", ***Semantic scholar***. 10 (2019).

17. Allen, R.B., "Material differences in equine cortical and trabecular bone", ***Semantic Scholar***. (2014).

18. Katsimbri, P., "The biology of normal bone remodelling". ***European journal of cancer care***,. 26(6), (2017).

19. Khurana, K., "Bone regeneration by tuning the drug release from the calcium phosphate scaffolds",. 29,***UPCommons***. (2017).

20. Boyle, W.J., W.S. Simonet, and D.L.J.N. Lacey, "Osteoclast differentiation and activation", ***Nature***. 423(6937): p. 337-342 (2003).

21. Siddiqui, J.A. and N.C.J.P. Partridge, "Physiological bone remodeling: systemic regulation and growth factor involvement", ***Translational Medicine***. 31(3): p. 233-245 (2016).

22. Henkel, J., "Bone tissue engineering in two preclinical ovine animal models", ***Queensland University of Technology***. p.18-18. (2017).

23. Kao, S.T. and D.D. Scott, "A review of bone substitutes". ***Oral and maxillofacial surgery clinics of North America***,. 19(4): p. 513-521 (2007).

24. Janicki, P. and G. Schmidmaier, "What should be the characteristics of the ideal bone graft substitute? Combining scaffolds with growth factors and/or stem cells". ***Nature***,. 42: p. S77-S81 (2011).

25. Moore, W.R., S.E. "Graves, and G.I. Bain, Synthetic bone graft substitutes". ***ANZ journal of surgery***,. 71(6): p. 354-361 (2001).

26. Srinath, P., P. Abdul Azeem, and K. "Venugopal Reddy, Review on calcium silicate-based bioceramics in bone tissue engineering". ***International Journal of Applied Ceramic Technology***,. 17(5): p. 2450-2464 (2020).

27. Goltzman, D. and G.N. Hendy, "The calcium-sensing receptor in bone—mechanistic and therapeutic insights". ***Nature Reviews Endocrinology***, 11(5): p. 298 (2015).

28. Breuksch, I., M. Weinert, and W. Brenner, "The role of extracellular calcium in bone metastasis". ***Journal of bone oncology***,. 5(3): p. 143-145 (2016).

29. Coleman, R. "Treatment of metastatic bone disease and the emerging role of radium". ***Seminars in nuclear medicine***., p.223. (2016).

30. Arora, M. and E. Arora, "The promise of silicon: bone regeneration and increased bone density". ***Journal of arthroscopy and joint surgery***,. 4(3): p. 103-105 (2017).

31. Millucci, L., Mariagiulia Minettia Maurizio Orlandinia., "Beer promotes differentiation and mineralization of human osteoblastic cells: Role of silicon". ***Journal of Functional Foods***,. **54**: p. 109-118 (2019).

32. Lowe, N.M., W.D. Fraser, and M.J.J.P.o.t.N.S. Jackson, "Is there a potential therapeutic value of copper and zinc for osteoporosis?", ***Proceedings of the Nutrition***. 61(2): p. 181-185, (2002).

33. Chihara, S. and J.J.D.-a.-m.D. Segreti, ***"*Osteomyelitis", *Brazilian Journal of Pharmaceutical Sciences*.** 56(1): p. 5-31 (2010).

34. Caputo, G.M., "Assessment and management of foot disease in patients with diabetes", ***National Center for Biotechnology Information Search database.*** 331(13): p. 854-860 (1994).

35. Jauregui, L., "Diagnosis and management of bone infections". ***Informa Health Care*** Vol. 16. (1995).

36. Ciampolini, J. and K.J.P.m.j. Harding, "Pathophysiology of chronic bacterial osteomyelitis Why do antibiotics fail so often?.", ***Microbial cell*** 76(898): p. 479-483 (2000).

37. Eid, A.J. and E.F.J.L.J.m.l.T.L.m.j. Berbari, "Osteomyelitis: review of pathophysiology", ***The Lebanese Medical Journal***. 60(1): p. 51-60 (2012).

38. De Jonghe, M. and G.J.B.d.l.S.d.S.M.d.G.-d.d.L. Glaesener, "Type B Haemophilus influenzae infections". ***Bulletin de la Societe des Sciences***. 132(2): p. 17-20 (1995).

39. Mader, J.T., "The host and the skeletal infection": ***Best Practice & Research Clinical Rheumatology***,. 13(1): p. 1-20 (1999).

40. Berendt, T. and I.J.C.m. Byren," Bone and joint infection", ***National Center for Biotechnology Information Search database.*** 4(6): p. 510 (2004).

41. Brady, R.A., "Osteomyelitis and the role of biofilms in chronic infection". ***FEMS Immunology & Medical Microbiology***,. 52(1): p. 13-22 (2008).

42. Lavery, L.A.," Microbiology of osteomyelitis in diabetic foot infections". ***The Journal of Foot and Ankle Surgery***,. 34(1): p. 61-64 (1995).

43. Price, G. and D.A. Patel, "Drug Bioavailability", ***Europe PMC plus***. p.59 (2020).

44. Tahara, Y. and Y.J.J.o.o.s. Ishii, "Apatite cement containing cis-diamminedichloroplatinum implanted in rabbit femur for sustained release of the anticancer", ***Journal of orthopaedic science***,. 6(6): p. 556-565 (2001).

45. Langer, R. and N.A.J.A.J. Peppas, "Advances in biomaterials, drug delivery, and bionanotechnology", ***AIChE Journal.*** 49(12): p. 2990-3006 (2003).

46. Acar, H.,"Molecular engineering solutions for therapeutic peptide delivery", ***Chemical sociey***. 46(21): p. 6553-6569 (2017).

47. Ramasamy, T., "Smart chemistry-based nanosized drug delivery systems for systemic application"s: A comprehensive review. ***Journal of Controlled Release***,. 258: p. 226-253 (2017).

48. Shi, J., Alexander R. Votruba, Omid C. Farokhzad, and Robert Langer., "Nanotechnology in drug delivery and tissue engineering": ***Nano letters***. 10(9): p. 3223-3230 (2010).

49. Park, K., "Controlled drug delivery systems": Past forward and future back. ***Journal of Controlled Release***,. 190: p. 3-8 (2014).

50. Rezaie, H.R., "A Review of Biomaterials and Their Applications in Drug Delivery",: ***Springer***. p.1-8., (2018).

51. McLean, A.J. and D.G.J.P.r., "Aging biology and geriatric clinical pharmacology". ***Le Couteur***, 56(2): p. 163-184 (2004).

52. Rothe, R., "Adjuvant Drug-Assisted Bone Healing: Advances and Challenges in Drug Delivery Approaches", ***Pharmaceutics***. 12(5): p. 428 (2020).

53. Vallet-Regí, M., "Mesoporous Silica Nanoparticles for Drug Delivery": ***Molecules.*** 23(1): p. 47 (2018).

54. Kwon, S., "Silica-based mesoporous nanoparticles for controlled drug delivery", ***Journal of Tissue Engineering***. 4: p. 2041731413503357 (2013).

55. Wang, S.J.M. and m., "Ordered mesoporous materials for drug delivery". ***Materials***. 117(1-2): p. 1-9 (2009).

56. Slowing, I.I.," Mesoporous silica nanoparticles as controlled release drug delivery and gene transfection carriers", ***Advanced Drug Delivery Reviews.*** 60(11): p. 1278-1288 (2008).

57. Wu, P. and D.W.J.B. Grainger, "Drug/device combinations for local drug therapies and infection prophylaxis", ***Biomaterials***. 27(11): p. 2450-2467 (2006).

58. Kwon, S., "Silica-based mesoporous nanoparticles for controlled drug delivery". ***Journal of Tissue Engineering***,. 4: p. 2041731413503357 (2013).

59. Dvir, T., "Nanotechnological strategies for engineering complex tissues", ***Nature nanotechnology***,. 6(1): p. 13-22 (2011).

60. Stanford, C.M., "Radiopacity of light-cured posterior composite resins". ***Journal of the American Dental Association***. 115(5): p. 722-4 (1987).

61. Hsu, J.C., "Nanoparticle contrast agents for X-ray imaging applications", ***Nanomedicine and Nanobiotechnology***. 12(6): p. e1642 (2020).

62. Islam, I., H.K. Chng, and A.U.J.J.J.o.e. Yap, "Comparison of the physical and mechanical properties of MTA and Portland cement", ***Nanomedicine and Nanobiotechnology***. 32(3): p. 193-197 (2006).

63. Kim, E.-C., "Evaluation of the radiopacity and cytotoxicity of Portland cements containing bismuth oxide", ***Oral Surgery, Oral Medicine, Oral Pathology, Oral Radiology, and Endodontology***. 105(1): p. e54-e57 (2008).

64. Ciobanu, G. and M. Harja, "Bismuth-Doped Nanohydroxyapatite Coatings on Titanium Implants for Improved Radiopacity and Antimicrobial Activity", ***Nanomaterials.*** 9(12): p. 1696 (2019).

65. Wu, T., "Preparation and cytocompatibility of a novel bismuth aluminate/calcium phosphate cement with high radiopacity". ***Journal of Materials Science: Materials in Medicine***,. 29(9): p. 149 (2018).

66. Ajeesh, M., "Nano iron oxide–hydroxyapatite composite ceramics with enhanced radiopacity", ***Journal of Materials Science***. 21(5): p. 1427-1434 (2010).

67. Pravina, P., D. Sayaji, and M. Avinash, "Calcium and its role in human body". ***International Journal of Research in Pharmaceutical and Biomedical Sciences***,. 4(2): p. 659-668 (2013).

68. Wu, S., "Biomimetic porous scaffolds for bone tissue engineering", ***Materials Science and Engineering***. 80: p. 1-36 (2014).

69. Chen, J.J.," Solubility and structure of calcium silicate hydrate", ***Cement and Concrete Research***. 34(9): p. 1499-1519 (2004).

70. Eltohamy, M., "Anti-bacterial zinc-doped calcium silicate cements: Bone filler", ***Ceramics International***,. 44(11): p. 13031-13038 (2018).

71. Atmeh, A., "Calcium silicate cement-induced remineralisation of totally demineralised dentine in comparison with glass ionomer cement: tetracycline labelling and two-photon fluorescence microscopy", ***Journal of Microscopy***. 257(2): p. 151-160 (2015).

72. Zhang, J., "Combination of simvastatin, calcium silicate/gypsum, and gelatin and bone regeneration in rabbit calvarial defects", ***Scientific Reports***.6(1): p. 1-12 (2016).

73. Gao, C., "Bone biomaterials and interactions with stem cells". ***Bone research***,. 5(1): p. 1-33 (2017).

74. Shirazi, F.S., "Mechanical and physical properties of calcium silicate/alumina composite for biomedical engineering applications". ***Journal of the Mechanical Behavior of Biomedical Materials***,. 30: p. 168-175 (2014).

75. Liu, X., "Bioactive calcium silicate ceramics and coatings". ***Biomedicine & Pharmacotherapy***,. 62(8): p. 526-529 (2008).

76. De Aza, P., F. Guitian, and S.J.S.m.e.m. De Aza, "Bioactivity of wollastonite ceramics: in vitro evaluation". ***Scripta metallurgica et materialia*** 31(8): p. 1001-1005 (1994).

77. Siriphannon, P., "Formation of hydroxyapatite on $CaSiO_3$ powders in simulated body fluid", ***Journal of the European***. 22(4): p. 511-520 (2002).

78. Engstrand, J., E. Unosson, and H.J.I.S.R.N. Engqvist, "Hydroxyapatite formation on a novel dental cement in human saliva",***International scholary.,*** p.4-., (2012).

79. Ni, S. and J.J.J.o.b.a. Chang, "In vitro degradation, bioactivity, and cytocompatibility of calcium silicate, dimagnesium silicate, and tricalcium phosphate bioceramics", ***Journal of biomaterials applications***24(2): p. 139-158, (2009).

80. Weissbart, E.J. and J.D.J.G.e.C.A. Rimstidt, "Wollastonite: Incongruent dissolution and leached layer formation", ***Geochimica et Cosmochimica Acta*** 64(23): p. 4007-4016 (2000).

81. Xue, W., A. Bandyopadhyay, and S.J.A.B. Bose, "Mesoporous calcium silicate for controlled release of bovine serum albumin protein", ***Acta Biomaterialia*** 5(5): p. 1686-1696 (2009).

82. Aza, D. and D.J.J.o.M. Aza, "Morphological and structural study of pseudowollastonite implants in bone", ***Journal of Microscopy*** 197(1): p. 60-67 (2000).

83. Catauro, M., "Synthesis of SiO_2 and CaO rich calcium silicate systems via sol-gel process: bioactivity, biocompatibility, and drug delivery tests", ***Research Part A*** 102(9): p. 3087-3092 (2014).

84. Wu, J., "Hierachically nanostructured mesoporous spheres of calcium silicate hydrate: Surfactant-free sonochemical synthesis and drug-delivery system with ultrahigh drug-loading capacity", ***Research Part A*** 22(6): p. 749-753 (2010).

85. Wu, J., "Amorphous calcium silicate hydrate/block copolymer hybrid nanoparticles: synthesis and application as drug carriers", ***Dalton Transactions*** 42(19): p. 7032-7040 (2013).

86. Zhu, W., "Exploitation of 3D face-centered cubic mesoporous silica as a carrier for a poorly water soluble drug: Influence of pore size on release rate". ***Materials Science and Engineering***: C,. 34: p. 78-85 (2014).

87. Zhu, Y.-J., X.-X. Guo, and T.-K.J.E.o.o.d.d. Sham, "Calcium silicate-based drug delivery systems", ***Expert opinion on drug delivery*** 14(2): p. 215-228 (2017).

88. Casey, W.H., "Leaching and reconstruction at the surfaces of dissolving chain-silicate minerals", ***Nature*** 366(6452): p. 253-256 (1993).

89. Tavares, M.T., "Platelet lysates-based hydrogels incorporating bioactive mesoporous silica nanoparticles for stem cell osteogenic differentiation", ***Materials Today Bio***,. 9: p. 100096, (2021).

90. Perez, R., "Therapeutic bioactive microcarriers: co-delivery of growth factors and stem cells for bone tissue engineering", ***Acta biomaterialia*** 10(1): p. 520-530 (2014).

91. Wu, C. and J.J.I.f. Chang, "Mesoporous bioactive glasses: structure characteristics, drug/growth factor delivery and bone regeneration application", ***Interface focus.*** 2(3): p. 292-306 (2012).

92. Zhu, Y., "Composition–structure–property relationships of the CaO–M x O y–SiO_2–P_2 O_5 (M= Zr, Mg, Sr) mesoporous bioactive glass (MBG) scaffolds", ***Journal of Material.*** 1. 21(25): p. 9208-9218 (2011).

93. Hench, L.L. and I.J.J.o.t.R.S.I. "Thompson, Twenty-first century challenges for biomaterials", ***Journal of the Royal Society***. **7**(suppl_4): p. S379-S391 (2010).

94. Lee, H.J., "Catechol-functionalized adhesive polymer nanoparticles for controlled local release of bone morphogenetic protein-2 from titanium surface", ***Journal of Controlled Release***. 170(2): p. 198-208 (2013).

95. Horcajada, P.,"Influence of pore size of MCM-41 matrices on drug delivery rate". ***Microporous and Mesoporous Materials***,. 68(1): p. 105-109 (2004).

96. Lee, Y.Y., "Photocatalytic CO_2 conversion on highly ordered mesoporous materials: comparisons of metal oxides and compound semiconductors", ***Applied Catalysis B: Environmental.*** 224: p. 594-601,(2018).

97. Chaudhary, V. and S.J.J.o.P.M. Sharma, "An overview of ordered mesoporous material SBA-15: synthesis, functionalization and application in oxidation reactions", ***Journal of Porous Materials***. 24(3): p. 741-749, (2017).

98. Henning, L.M., LM Henning, DD Cubas, MG Colmenares. "High specific surface area ordered mesoporous silica COK-12 with tailored pore size", ***Microporous and Mesoporous Materials***. 280: p. 133-143, (2019).

99. Zheng, A., Ao Zhengab Lingyan Caoab Yang Liuc Jiannan Wuab. "Biocompatible silk/calcium silicate/sodium alginate composite scaffolds for bone tissue engineering", ***Carbohydrate polymer*** 199: p. 244-255, (2018).

100. Guo, X., aoxuan Guo, Zhiqiang Wang, Jin Wu, Yun-Mui Yiu. "Tracking drug loading capacities of calcium silicate hydrate carrier: a comparative X-ray absorption near edge structures study", ***Physical chemistry***. 119(31): p. 10052-10059 (2015).

101. Fan, Y., Shanshan Huanga Jinhua Jiangb Guogang Li. "Luminescent, mesoporous, and bioactive europium-doped calcium silicate (MCS: Eu^{3+}) as a drug carrier. Journal of Colloid and Interface Science", ***Journal of Colloid and Interface Science***. 357(2): p. 280-285, (2011).

102. Kang, X., X Kang, S Huang, P Yang, D Yang, J Lin., "Preparation of luminescent and mesoporous Eu^{3+}/Tb^{3+} doped calcium silicate microspheres as drug carriers via a template route". ***Dalton Transactions***,. 40(9): p. 1873-1879 (2011).

103. Meng, Q., J Lin, L Fu, H Zhang, S Wang., "Sol–gel deposition of calcium silicate red-emitting luminescent films doped with Eu^{3+}", ***Journal of Materials***. 11(12): p. 3382-3386 (2001).

104. Peng, X.-Y., "La-Doped mesoporous calcium silicate/chitosan scaffolds for bone tissue engineering". ***Biomaterials science***,. 7(4): p. 1565-1573 (2019).

105. El Nahrawy, A., "Synthesis and Characterization of Hybrid Chitosan/Calcium Silicate Nanocomposite Prepared Using Sol-Gel Method". ***Biomaterials science***,. 2(1): p. 9-14 (2015).

106. Taghvaei, A.H., "Synthesis and characterization of novel mesoporous strontium-modified bioactive glass nanospheres for bone tissue engineering applications", ***Microporous and Mesoporous Materials***. 294: p. 109889 (2020).

107. Riti, P.I., "The effect of synthesis route and magnesium addition on structure and bioactivity of sol–gel derived calcium-silicate glasses", ***Ceramics International***,. 40(9, Part B): p. 14741-14748 (2014).

108. Kamali, M. and A.J.S.r. " Effect of biomolecules on the nanostructure and nanomechanical property of calcium-silicate-hydrate", ***Ghahremaninezhad***. 8(1): p. 1-16 (2018).

109. Dong, Y., "Preparation and Drug Release Properties of IBU-Loaded Mesoporous Calcium Silicate Hydrate (CSH) Spheres". ***in Advanced Materials Research***., p.894-897., (2012).

110. Beheri, H.H., "Mechanical and microstructure of reinforced hydroxyapatite/calcium silicate nano-composites materials", ***Materials & Design.*** 44: p. 461-468 (2013).

111. Cao, J., "Hydrothermal synthesis of xonotlite from carbide slag", ***Progress in Natural Science***. 18(9): p. 1147-1153 (2008).

112. ARSLAN, Y., "The Effect of Synthesis Conditions on Calcium Silicate Bioceramic Materials", ***Fen Bilimleri Enstitüsü Dergisi***. 23(3): p. 727-737 (2019).

113. ÇARDAKLI., "Lanthanum Oxide Doped Calcium Silicates Particles: Preparation and Characterization", ***Fen Bilimleri Enstitüsü Dergisi***, . 25(2): p. 255-261 (2021).

114. Barve, R.A.,., "Optical properties and Judd–Ofelt analysis of Eu^{3+} activated calcium silicate". ***Physica B: Condensed Matter***,. 475: p. 156-161 (2015).

115. Zaichick, S., "Accumulation of rare earth elements in human bone within the lifespan". ***Metallomics***,. 3(2): p. 186-194 (2011).

116. Xu, B., "Experimental and theoretical study of hydrogen atom abstraction from n-butane by lanthanum oxide cluster anions", ***Physical chemistry***. 115(37): p. 10245-10250 (2011).

117. Jabeen, F., "Silica–lanthanum oxide: pioneer composite of rare-earth metal oxide in selective phosphopeptides enrichment", ***Analytical chemistry***. 84(23): p. 10180-10185 (2012).

118. Veerasingam, M., B. Murugesan, and S.J.J.o.R.E. Mahalingam, "Ionic liquid mediated morphologically improved lanthanum oxide nanoparticles by Andrographis paniculata leaves extract and its biomedical applications" ***Journal of Rare Earths***. 38(3): p. 281-291 (2020).

119. Bhagya Mathi, D., D. Gopi, and L. Kavitha, "Implication of lanthanum substituted hydroxyapatite/poly(n-methyl pyrrole) bilayer coating on titanium for orthopedic applications". ***Materials Today: Proceedings***,. 26: p. 3526-3530 (2020).

120. Singh, A.K.J.I.A.D. and P.i. Asia, 14 "Production and discovery of documents in arbitration in India" ***International Arbitration Discourse and Practices in Asia***. P. 176-185 (2017).

121. De, D., "Antibacterial effect of lanthanum calcium manganate (La0. 67Ca0. 33MnO3) nanoparticles against Pseudomonas aeruginosa ATCC 27853", ***Journal of Biomedical Nanotechnology.*** 6(2): p. 138-144. (2010).

122. Balusamy, B., "Characterization and bacterial toxicity of lanthanum oxide bulk and nanoparticles". ***Journal of Rare Earths***,. 30(12): p. 1298-1302 (2012).

123. Motameni, A., "Structural and Biological Analysis of Mesoporous Lanthanum Doped βTCP For Potential Use as Bone Graft Material". ***Materials Today Communications***. 23: p. 101151 (2020).

124. Guo, D.G., "Characterization, physicochemical properties and biocompatibility of La-incorporated apatites". ***Acta Biomaterialia***,. 5(9): p. 3512-3523 (2009).

125. Bulina, N.V., "Lanthanum–silicate–substituted apatite synthesized by fast mechanochemical method: Characterization of powders and biocoatings produced by micro–arc oxidation". ***Materials Science and Engineering***: C, .. 92: p. 435-446 (2018).

126. Brabu, B., "Biocompatibility studies on lanthanum oxide nanoparticles". ***Toxicology Research***,. 4(4): p. 1037-1044 (2015).

127. Lou, W., "Preparation and Characterization of Lanthanum-Incorporated Hydroxyapatite Coatings on Titanium Substrates". ***International Journal of Molecular Sciences***,. 16(9): p. 21070-21086 (2015).

128. Thompson, K.H. and C. Orvig, Editorial: "Lanthanide compounds for therapeutic and diagnostic applications", ***Chemical Society Reviews***,. **35**(6): p. 499-499 (2006).

129. Cui, H., "Facile synthesis of Mg-doped calcium silicate porous nanoparticles for targeted drug delivery and ovarian cancer treatment". ***Ceramics International***,.47(17): p.24942-24948., (2021).

130. Joshy, M.A., "*In vitro* sustained release of amoxicillin from lanthanum hydroxyapatite nano rods". ***Current Applied Physics***,. 11(4): p. 1100-1106 (2011).

131. Gautam, C., "Synthesis, structural and 3-D architecture of lanthanum oxide added hydroxyapatite composites for bone implant applications: Enhanced microstructural and mechanical properties". ***Ceramics International***,. 43(16): p. 14114-14121 (2017).

132. Jadalannagari, S., "Lanthanum-doped hydroxyapatite nanoparticles as biocompatible fluorescent probes for cellular internalization and biolabeling", ***Science of Advanced Materials,***. 6(2): p. 312-319 (2014).

133. El-Meliegy, E., "Evaluation of solubility and cytotoxicity of lanthanum-doped phosphate glasses nanoparticles for drug delivery applications", ***Journal of Non-Crystalline Solids***. 475: p. 59-70 (2017).

134. No, Y.J., "Strontium-doped calcium silicate bioceramic with enhanced in vitro osteogenic properties***", Biomedical Materials***. 12(3): p. 035003 (2017).

135. Lin, K., "Enhanced osteoporotic bone regeneration by strontium-substituted calcium silicate bioactive ceramics". ***Biomaterials***,. 34(38): p. 10028-10042 (2013).

136. Zreiqat, H., "The incorporation of strontium and zinc into a calcium–silicon ceramic for bone tissue engineering". ***Biomaterials***,. 31(12): p. 3175-3184 (2010).

137. Cui, H., "Facile synthesis of Mg-doped calcium silicate porous nanoparticles for targeted drug delivery and ovarian cancer treatment", ***Ceramics International***,. p.24942-24948, (2021).

138. Kee, C.C., B.C. Ang, and H.S.C. "Metselaar, Synthesis of europium-doped calcium silicate hydrate via hydrothermal and coprecipitation method". ***Ceramics International***,. 47(4): p. 4803-4812 (2021).

139. Wang, D., S. Han, and B.-B. Lu, "Biocompatible Eu doped mesoporous calcium silicate nanospheres for pH-responsive drug release". ***Inorganic Chemistry Communications***,. 133: p. 108872 (2021).

140. Zhu, Y., "Substitutions of strontium in mesoporous calcium silicate and their physicochemical and biological properties", ***Acta Biomaterialia***,. 9(5): p. 6723-6731 (2013).

141. Mabrouk, M., "Cancer Cells Treated by Clusters of Copper Oxide Doped Calcium Silicate", ***Advanced Pharmaceutical Bulletin***. 9: p. 102 - 109 (2019).

142. Du, Z., "Calcium silicate scaffolds promoting bone regeneration via the doping of Mg^{2+} or Mn^{2+} ion", ***Composites Part B: Engineering***. 190: p. 107937 (2020).

143. Hang, C., "Mesoporous LaB6@calcium silicate composite: Preparation, NIR photothermal conversion and drug delivery properties". ***Ceramics International***,. 44(7): p. 8427-8434 (2018).

144. Pouroutzidou, G.K., "Synthesis and Characterization of Mesoporous Mg-and Sr-Doped Nanoparticles for Moxifloxacin Drug Delivery in Promising Tissue Engineering Applications" , ***International Journal of Molecular Sciences***. 22(2): p. 577 (2021).

145. Lakshmi, R. and S.J.I.j.o.n. Sasikumar, "Influence of needle-like morphology on the bioactivity of nanocrystalline wollastonite–an in vitro study", ***International journal of nanomedicine***. 10(Suppl 1): p. 129 (2015).

146. Adams, L.A., E.R. Essien, and E.E.J.J.o.A.C.S. Kaufmann, "A new route to sol-gel crystalline wollastonite bioceramic", ***Journal of Asian Ceramic***. 6(2): p. 132-138 (2018).

147. Jesser, W. and D.J.p.s.s., "On the theory of interfacial energy and elastic strain of epitaxial overgrowths in parallel alignment on single crystal substrates", ***Kuhlmann-Wilsdorf***,. 19(1): p. 95-105 (1967).

148. Rameshbabu, N., "Antibacterial nanosized silver substituted hydroxyapatite: synthesis and characterization", ***Journal of Biomedical Material Research Part A.*** . 80(3): p. 581-591 (2007).

149. Chakradhar, R.S., "Solution combustion derived nanocrystalline macroporous wollastonite ceramics", ***Materials Chemistry and Physics***. 95(1): p. 169-175 (2006).

150 Saravanan, S., "Role of mesoporous wollastonite (calcium silicate) in mesenchymal stem cell proliferation and osteoblast differentiation: a cellular and molecular study***", Journal of Biomedical Nanotechnology***. 11(7): p. 1124-1138 (2015).

151. Ismail, H., R. Shamsudin, and M.A. Abdul Hamid, "Effect of autoclaving and sintering on the formation of β-wollastonite", ***Materials Science and Engineering: C,***. 58: p. 1077-1081 (2016).

152. Kolhe, P. and R.M.J.B. Kannan, "Improvement in ductility of chitosan through blending and copolymerization with PEG: FTIR investigation of molecular interactions***", Biomacromolecules*** . 4(1): p. 173-180 (2003).

153. Paluszkiewicz, C., "Nucleation of hydroxyapatite layer on wollastonite material surface: FTIR studies", ***Vibrational Spectroscopy***. (2008). 48(2): p. 263-268 (2008).

154. Meiszterics, A., "Structural characterization of gel-derived calcium silicate systems", ***Physical chemistry***. 114(38): p. 10403-10411 (2010).

155. Reddy, M.V., et al., "*In Vitro* Biological Evaluations of Zn Doped $CaSiO_3$ Synthesized by Sol–Gel Combustion Technique", ***Journal of Inorganic and Organometallic Polymers.*** 28(6): p. 2187-2195 (2018).

156. Saravanapavan, P. and L.L. Hench, "Mesoporous calcium silicate glasses. I. Synthesis", ***Journal of Non-Crystalline Solids***,. 318(1): p. 1-13 (2003).

157. Tangboriboon, N., "An innovative $CaSiO_3$ dielectric material from eggshells by sol–gel process", ***Journal of Sol-Gel Science and Technology.*** 58(1): p. 33-41 (2011).

158. Böke, H., "Quantification of $CaCO_3$–$CaSO_3 \cdot 0.5\ H_2O$–$CaSO_4 \cdot 2H_2O$ mixtures by FTIR analysis and its ANN model", ***Materials Letters***. 58(5): p. 723-726 (2004).

159. Lakshmi, R., "Preparation and phase evolution of wollastonite by sol-gel combustion method using sucrose as the fuel"**,** ***Combustion Science and Technology.*** *185(12):* p. 1777-1785 (2013).

160. Alshemary, A.Z.,"Nanocrystalline Zn^{2+} and SO_4^{2-} binary doped fluorohydroxyapatite: A novel biomaterial with enhanced osteoconductive and osteoinconductive properties", ***Materials Science and Engineering:*** *C,*. 104: p. 109884 (2019).

161. Xiao, S., "Immobilization of the cell-adhesive peptide Arg–Gly–Asp–Cys (RGDC) on titanium surfaces by covalent chemical attachment", ***Journal of Materials Science: Materials in Medicine.*** 8(12): p. 867-872 (1997).

162. Dong, G., "The effect of silicon doping on the transformation of amorphous calcium phosphate to silicon-substituted α-tricalcium phosphate by heat treatment" ***Ceramics International,***. 42(1, Part A): p. 883-890 (2016).

163. Lu, H.B., "Surface characterization of hydroxyapatite and related calcium phosphates by XPS and TOF-SIMS", ***Analytical chemistry***. 72(13): p. 2886-2894 (2000).

164. Shi, C., "Porous chitosan/hydroxyapatite composite membrane for dyes static and dynamic removal from aqueous solution", ***Journal of hazardous materials.*** **338**: p. 241-249 (2017).

165. You, Y., "Sodium alginate templated hydroxyapatite/calcium silicate composite adsorbents for efficient dye removal from polluted water", ***International Journal of Biological Macromolecules***. 141: p. 1035-1043 (2019).

166. Yousuf, M., "An FTIR and XPS investigations of the effects of carbonation on the solidification/stabilization of cement based systems-Portland type V with zinc", ***Cement and Concrete Research***. 23(4): p. 773-784 (1993).

167. Black, L., "X-ray photoelectron spectroscopic investigation of nanocrystalline calcium silicate hydrates synthesised by reactive milling", ***Cement and Concrete Research***. 36(6): p. 1023-1031 (2006).

168. Black, L., "Characterisation of crystalline CSH phases by X-ray photoelectron spectroscopy", ***Cement and Concrete Research***. 33(6): p. 899-911 (2003).

169. Bai, Y., "Preparation and characterization of reduced graphene oxide/fluorhydroxyapatite composites for medical implants", ***Journal of Alloys and Compounds***,. 688: p. 657-667 (2016).

170. Black, L., "Characterisation of crystalline C-S-H phases by X-ray photoelectron spectroscopy", ***Cement and Concrete Research***,. 33(6): p. 899-911 (2003).

171. Motameni, A., "Structural and biological analysis of mesoporous lanthanum doped βTCP for potential use as bone graft material", ***Materials Today Communications***. 23: p. 101151 (2020).

172. Mahmood, B.K., "Effects of strontium - erbium co-doping on the structural properties of hydroxyapatite: An Experimental and theoretical study", ***Ceramics International***,. 46(10, Part B): p. 16354-16363 (2020).

173. Goh, Y.-F., "*In-vitro* characterization of antibacterial bioactive glass containing ceria" ***Ceramics International***, (2014). 40(1, Part A): p. 729-737.

174. Yi, K., "The adsorption and transformation of SO_2, H_2S and NH_3 by using sludge gasification ash: Effects of Fenton oxidation and CaO pre-conditioning", ***Chemical Engineering Journal***. 360: p. 1498-1508(2019).

175. Huang, W., "Lanthanum-doped ordered mesoporous hollow silica spheres as novel adsorbents for efficient phosphate removal', ***Journal of Materials Chemistry A***. 2(23): p. 8839-8848 (2014).

176. Gallinetti, S., C. Canal, and M.P.J.J.o.t.A.C.S., "Development and Characterization of Biphasic Hydroxyapatite/β-TCP Cements", ***Journal of the American Ceramic Society.*** 97(4): p. 1065-1073 (2014).

177. Senamaud, N., "Calcination and sintering of hydroxyfluorapatite powders". ***Solid State Ionics***,. 101-103: p. 1357-1362 (1997).

178. Bilgin, s., "Injectable alginate/dicalcium phosphate cement composites for bone tissue engineering", ***Karabuk University.*** (2020).

179. Singh, K., R. Kumar, and A. "Chowdhury, Lanthanum doped Ceria Nanoparticles: a Promising Material for Energy Applications", ***Materials Today: Proceedings***,. 5(11, Part 2): p. 22993-22997 (2018).

180. Yamaguchi, N., "Synthesis of CaO-SiO_2 Compounds Using Materials Extracted from Industrial Wastes", ***Open Journal of Inorganic Non-metallic Materials.*** 5(01): p. 1 (2014).

181. Peña-Poza, J., "Lanthanum-Silica Sol-Gel Coatings for Protecting Metallic Materials in Museums: Approaches to Copper, Bronze, Lead and Steel", ***Coatings Journal***. 8(4): p. 138 (2018).

182. Camilleri, J. and M.G. Gandolfi, "Evaluation of the radiopacity of calcium silicate cements containing different radiopacifiers", ***International Endodontic Journal.*** 43(1): p. 21-30 (2010).

183. Watts, D. and J.J.J.o.d. McCabe, "Aluminium radiopacity standards for dentistry: an international survey", ***Journal of dentistry***. 27(1): p. 73-78, (1999).

184. Tanomaru, J.M.G., "Radiopacity, pH and antimicrobial activity of Portland cement associated with micro-and nanoparticles of zirconium oxide and niobium oxide", ***Dental materials***. p. 2013-328 (2014).

185. Saliba, E., "Evaluation of the strength and radiopacity of Portland cement with varying additions of bismuth oxide", ***Journal of Endodontics***. 42(4): p. 322-328 (2009).

186. Colville, A.A., K.J.A.M.J.o.E., "A refinement of the structure of barite", ***Materials***. 52(11-12): p. 1877-1880 (1967).

187. Chen, C., "Radiopacity and cytotoxicity of Portland cement containing zirconia doped bismuth oxide radiopacifiers", ***Journal of Endodontics***. 40(2): p. 251-254 (2014).

188. Duarte, M.A.H., "Radiopacity of portland cement associated with different radiopacifying agents", ***Journal of Endodontics***. 35(5): p. 737-740 (2009).

189. Aguilar, F.G., "Radiopacity evaluation of calcium aluminate cement containing different radiopacifying agents", ***Journal of Endodontics***. 37(1): p. 67-71 (2011).

190. Alérico, M.S., "Effect of image acquisition parameters on the radiopacity of bulk-fill and nanocomposite resins", ***Oral Surgery, Oral Medicine, Oral Pathology and Oral Radiology***,. 132(2): p. 217-224 (2021).

191. Watts, D. and J.J.J.o.d., "Aluminium radiopacity standards for dentistry: an international survey", ***Journal of dentistry***. 27(1): p. 73-78 (1999).

192. Yang, X., "Multi-functionalized graphene oxide based anticancer drug-carrier with dual-targeting function and pH-sensitivity", ***Journal of Materials Chemistry***. 21(10): p. 3448-3454, (2011).

193. Gou, Z., "Study on the self-setting property and the in vitro bioactivity of β-Ca2SiO4",***Journal of Biomedical Materials Research Part B***. 73(2): p. 244-251 (2005).

194. Wu, C., J. Chang, and W. Fan, "Bioactive mesoporous calcium–silicate nanoparticles with excellent mineralization ability, osteostimulation, drug-delivery and antibacterial properties for filling apex roots of teeth". ***Journal of Materials Chemistry***,. 22(33): p. 16801-16809 (2012).

195. Singh, G., S.S. Jolly, and R.P. Singh, "Cerium substituted hydroxyapatite mesoporous nanorods: Synthesis and characterization for drug delivery applications". ***Materials Today: Proceedings***,. 28: p. 1460-1466 (2020).

196. Balas, F., "Confinement and Controlled Release of Bisphosphonates on Ordered Mesoporous Silica-Based Materials". ***Journal of the American Chemical Society***,. 128(25): p. 8116-8117 (2006).

197. Manzano, M. and M.J.J.o.M.C. "Vallet-Regí, New developments in ordered mesoporous materials for drug delivery", ***Journal of Materials Chemistry***. 20(27): p. 5593-5604 (2010).

198. Vallet-Regi, M., "A new property of MCM-41: drug delivery system", ***Chemistry of Materials***. 13(2): p. 308-311 (2001).

199. Christy, A.A. "The nature of silanol groups on the surfaces of silica, modified silica and some silica based materials", ***Advanced Materials Research***., p. 3-10, (2014).

200. Liu, W., J.J.M.S. Chang, and E. C, "*In vitro* evaluation of gentamicin release from a bioactive tricalcium silicate bone cement", ***Materials Science and Engineering: C,.*** 29(8): p. 2486-2492 (2009).

201. Baker, R.W., "Controlled release of biologically active agents*"*, ***John Wiley & Sons***,(1987).

202. Lee, J.H. and Y. Yeo, "Controlled Drug Release from Pharmaceutical Nanocarriers", ***Chemical engineering science***. Chemical engineering science,. 125: p. 75-84, , (2015).

APPENDIX A.

CALIBRATION CURVE

Calibration Curve of Cmpicillin

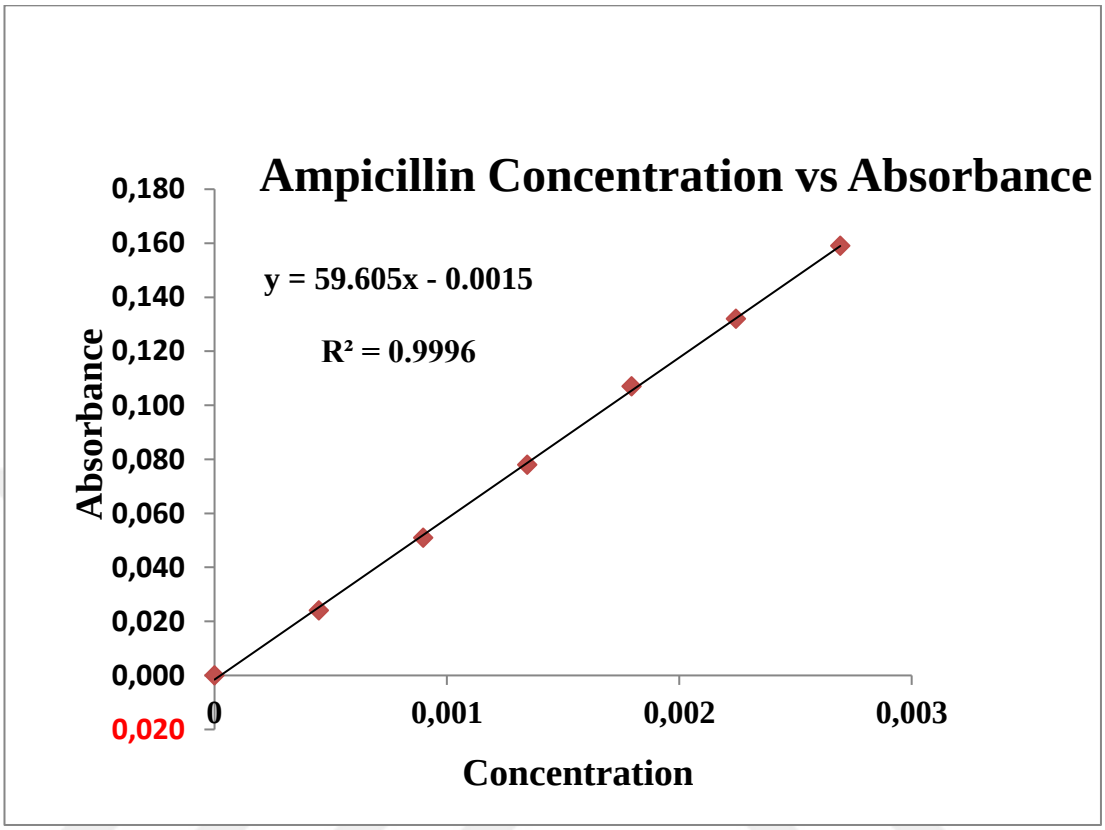

Calibration Curve of Gentamicin

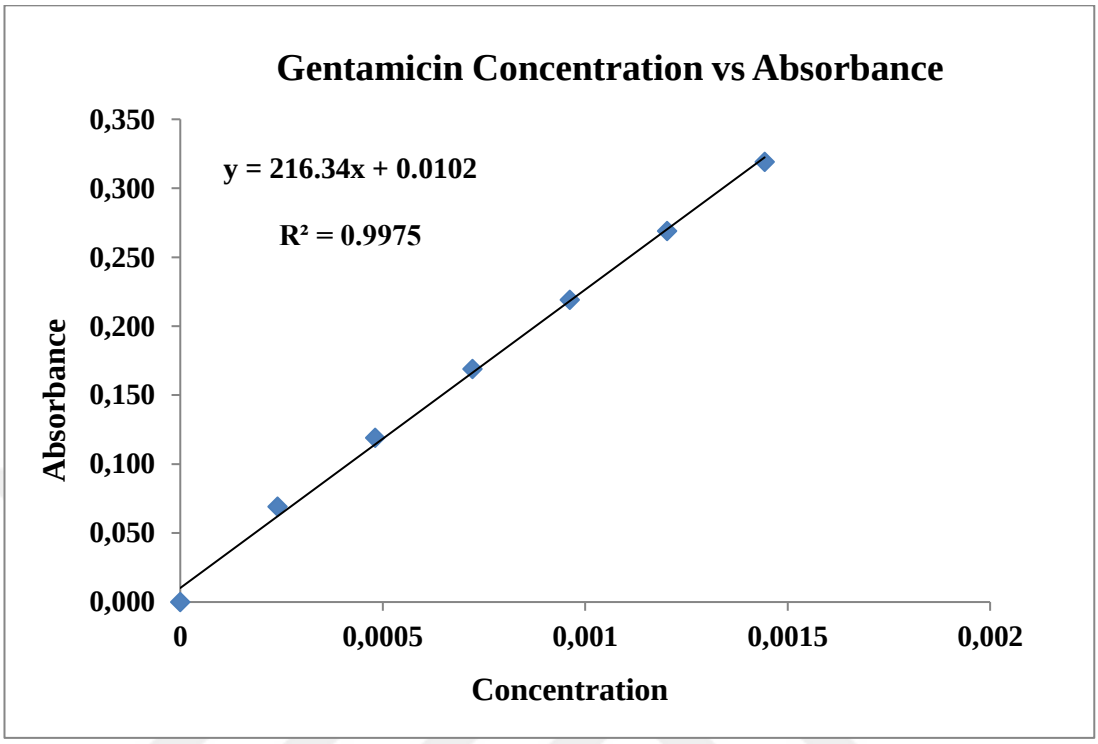

Calibration Curve of Cephalexin

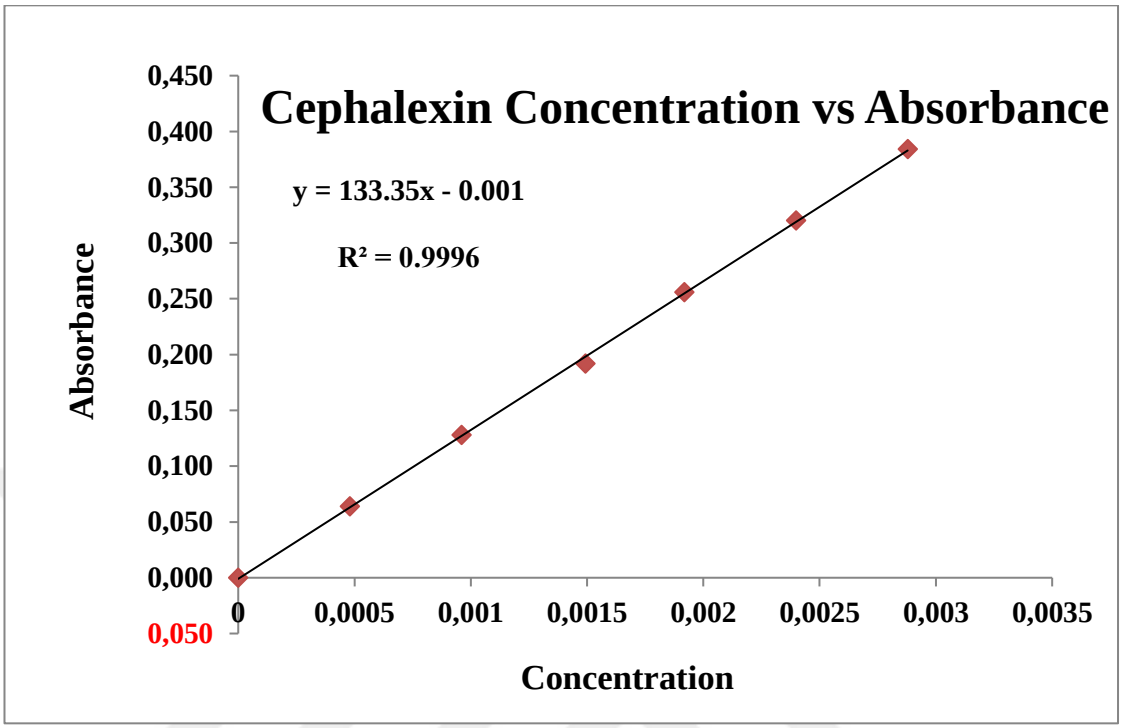

APPENDIX B.

CALIBRATION CURVE

Calculation of Absorbance and Drug Concentration Loading of Ampicillin

Sample	First Draw			Blanc	Abs 1	Abs 2	Abs3	Ampicillin loading		
	Sample1	Sample2	Sample3	Blanc	Abs1	Abs 2	Abs3	Conc1	Conc2	Conc3
CS	3.336	3.335	3.348	3.21	0.126	0.125	0.138	0.00214	0.00212	0.00234
1La	3.339	3.322	3.341	3.21	0.129	0.112	0.131	0.00219	0.00190	0.00222
2La	3.317	3.358	3.352	3.21	0.107	0.148	0.142	0.00182	0.00251	0.00241
3La	3.343	3.351	3.353	3.21	0.133	0.141	0.143	0.00226	0.00239	0.00242
Sample	Second Draw			Blanc	Abs 1	Abs 2	Abs3	Ampicillin loading		
	Sample1	Sample2	Sample3	Blanc	Abs1	Abs 2	Abs3	Conc1	Conc2	Conc3
CS	3.293	3.33	3.333	3.21	0.083	0.12	0.123	0.00142	0.00204	0.00209
1La	3.321	3.301	3.337	3.21	0.111	0.091	0.127	0.00189	0.00155	0.00216
2La	3.315	3.339	3.348	3.21	0.105	0.129	0.138	0.00179	0.00219	0.00234
3La	3.325	3.341	3.375	3.21	0.115	0.131	0.165	0.00195	0.00222	0.00279
Sample	Third Draw			Blanc	Abs1	Abs2	Abs3	Ampicillin loading		
	Sample1	Sample2	Sample3	Blanc	Abs1	Abs2	Abs3	Conc1	Conc2	Conc3
CS	3.264	3.326	3.326	3.21	0.054	0.116	0.116	0.00093	0.00197	0.00197
1La	3.301	3.292	3.331	3.21	0.091	0.082	0.121	0.00155	0.00140	0.00206
2La	3.311	3.331	3.339	3.21	0.101	0.121	0.129	0.00172	0.00206	0.00219
3La	3.316	3.333	3.341	3.21	0.106	0.123	0.131	0.00180	0.00209	0.00222

Calculation of Absorbance and Drug concentration Releasing of Ampicillin

Sample	Third Draw			Blanc	Abs1	Abs2	Abs3	Ampicillin release		
	Sample1	Sample2	Sample3	Blanc	Abs1	Abs2	Abs3	Conc1	Conc2	Conc3
CS	3.249	3.322	3.311	3.21	0.039	0.112	0.101	0.00068	0.00190	0.00172
1La-cs	3.297	3.273	3.327	3.21	0.087	0.063	0.117	0.00148	0.00108	0.00199
2La-cs	3.293	3.32	3.331	3.21	0.083	0.11	0.121	0.00142	0.00187	0.00206
3La-cs	3.303	3.321	3.336	3.21	0.093	0.111	0.126	0.00159	0.00189	0.00214
Sample	Second draw			Blanc	Abs 1	Abs 2	Abs3	Ampicillin release		
	Sample1	Sample2	Sample3	Blanc	Abs 1	Abs 2	Abs3	Conc1	Conc2	Conc3
CS	3.238	3.317	3.301	3.21	0.028	0.107	0.091	0.00049	0.00182	0.00155
1La-cs	3.247	3.265	3.324	3.21	0.037	0.055	0.114	0.00065	0.00095	0.00194
2La-cs	3.283	3.313	3.327	3.21	0.073	0.103	0.117	0.00125	0.00175	0.00199
3La-cs	3.289	3.311	3.33	3.21	0.079	0.101	0.12	0.00135	0.00172	0.00204
Sample	Third Draw			Blanc	Abs 1	Abs 2	Abs3	Ampicillin release		
	Sample1	Sample2	Sample3	Blanc	Abs 1	Abs 2	Abs 3	Conc1	Conc2	Conc3
CS	3.227	3.312	3.292	3.21	0.017	0.102	0.082	0.00031	0.00174	0.00140
1La-cs	3.242	3.251	3.311	3.21	0.032	0.041	0.101	0.00056	0.00071	0.00172
2La-cs	3.27	3.29	3.321	3.21	0.06	0.08	0.111	0.00103	0.00137	0.00189
3La-cs	3.276	3.298	3.324	3.21	0.066	0.088	0.114	0.00113	0.00150	0.00194

Calculation of Absorbance and Drug concentration Loading of Gentamicin

Sample	First Draw			Blanc	Abs 1	Abs 2	Abs3	Gentamicin loading		
	Sample1	Sample2	Sample3	Blanc	Abs 1	Abs 2	Abs3	Conc1	Conc2	Conc3
CS	3.484	3.451	3.463	3.321	0.163	0.13	0.142	0.00071	0.00055	0.00061
1La-cs	3.491	3.484	3.453	3.321	0.17	0.163	0.132	0.00074	0.00071	0.00056
2La-cs	3.474	3.444	3.521	3.321	0.153	0.123	0.2	0.00066	0.00052	0.00088
3La-cs	3.477	3.459	3.511	3.321	0.156	0.138	0.19	0.00067	0.00059	0.00083
Sample	Second draw			Blanc	Abs1	Abs 2	Abs 3	Gentamicin loading		
	Sample1	Sample2	Sample3	Blanc	Abs 1	Abs 2	Abs 3	Conc1	Conc2	Conc3
CS	3.459	3.447	3.458	3.321	0.138	0.126	0.137	0.00059	0.00054	0.00059
1La-cs	3.483	3.479	3.448	3.321	0.162	0.158	0.127	0.0007	0.00068	0.00054
2La-cs	3.469	3.439	3.503	3.321	0.148	0.118	0.182	0.00064	0.0005	0.00079
3La-cs	3.471	3.451	3.497	3.321	0.15	0.13	0.176	0.00065	0.00055	0.00077
Sample	Second draw			Blanc	Abs 1	Abs 2	Abs 3	Gentamicin loading		
	Sample1	Sample2	Sample3	Blanc	Abs 1	Abs 2	Abs 3	Conc1	Conc2	Conc3
CS	3.453	3.435	3.451	3.321	0.132	0.114	0.13	0.00056	0.00048	0.00055
1La-cs	3.479	3.476	3.444	3.321	0.158	0.155	0.123	0.00068	0.00067	0.00052
2La-cs	3.463	3.432	3.493	3.321	0.142	0.111	0.172	0.00061	0.00047	0.00075
3La-cs	3.466	3.445	3.491	3.321	0.145	0.124	0.17	0.00062	0.00053	0.00074

Calculation of Absorbance and Drug concentration Releasing of Gentamicin

Sample	First Draw			Blanc	Abs 1	Abs 2	Abs3	Gentamicin release		
	Sample1	Sample2	Sample3	Blanc	Abs 1	Abs 2	Abs3	Conc1	Conc2	Conc3
CS	3.442	3.403	3.423	3.321	0.121	0.082	0.102	0.00051	0.00033	0.00042
1La	3.449	3.443	3.413	3.321	0.128	0.122	0.092	0.00054	0.00052	0.00038
2La	3.445	3.401	3.459	3.321	0.124	0.08	0.138	0.00053	0.00032	0.00059
3La	3.441	3.413	3.453	3.321	0.12	0.092	0.132	0.00051	0.00038	0.00056
Sample	Second draw			Blanc	Abs1	Abs 2	Abs 3	Gentamicin release		
	Sample1	Sample2	Sample3	Blanc	Abs 1	Abs 2	Abs 3	Conc1	Conc2	Conc3
CS	3.437	3.396	3.414	3.321	0.116	0.075	0.093	0.00049	0.0003	0.00038
1La	3.442	3.432	3.41	3.321	0.121	0.111	0.089	0.00051	0.00047	0.00036
2La	3.433	3.396	3.436	3.321	0.112	0.075	0.115	0.00047	0.0003	0.00048
3La	3.429	3.399	3.447	3.321	0.108	0.078	0.126	0.00045	0.00031	0.00054
Sample	Second draw			Blanc	Abs 1	Abs 2	Abs 3	Gentamicin release		
	Sample1	Sample2	Sample3	Blanc	Abs 1	Abs 2	Abs 3	Conc1	Conc2	Conc3
CS	3.428	3.391	3.399	3.321	0.107	0.07	0.078	0.00045	0.00028	0.00031
1La	3.435	3.425	3.396	3.321	0.114	0.104	0.075	0.00048	0.00043	0.0003
2La	3.421	3.391	3.428	3.321	0.1	0.07	0.107	0.00042	0.00028	0.00045
3La	3.418	3.392	3.435	3.321	0.097	0.071	0.114	0.0004	0.00028	0.00048

Calculation of Absorbance and Drug Concentration Loading of Cephalexin

Sample	First Draw			Blanc	Abs 1	Abs 2	Abs3	Gentamicin releasing		
	Sample1	Sample2	Sample3	Blanc	Abs 1	Abs 2	Abs3	Conc1	Conc2	Conc3
CS	0.825	0.865	0.755	0.53	0.295	0.335	0.225	0.00222	0.00252	0.00169
1La	0.748	0.736	0.748	0.53	0.218	0.206	0.218	0.00164	0.00155	0.00164
2La	0.771	0.698	0.684	0.53	0.241	0.168	0.154	0.00181	0.00127	0.00116
3La	0.753	0.781	0.683	0.53	0.223	0.251	0.153	0.00168	0.00189	0.00115
Sample	Second draw			Blanc	Abs1	Abs 2	Abs 3	Gentamicin releasing		
	Sample1	Sample2	Sample3	Blanc	Abs 1	Abs 2	Abs 3	Conc1	Conc2	Conc3
CS	0.785	0.859	0.748	0.53	0.255	0.329	0.218	0.00192	0.00247	0.00164
1La	0.739	0.728	0.741	0.53	0.209	0.198	0.211	0.00157	0.00149	0.00159
2La	0.764	0.691	0.679	0.53	0.234	0.161	0.149	0.00176	0.00121	0.00112
3La	0.741	0.77	0.678	0.53	0.211	0.24	0.148	0.00159	0.00181	0.00112
Sample	Second draw			Blanc	Abs 1	Abs 2	Abs 3	Gentamicin releasing		
	Sample1	Sample2	Sample3	Blanc	Abs 1	Abs 2	Abs 3	Conc1	Conc2	Conc3
CS	0.776	0.851	0.742	0.53	0.246	0.321	0.212	0.00185	0.00241	0.0016
1La	0.726	0.713	0.735	0.53	0.196	0.183	0.205	0.00148	0.00138	0.00154
2La	0.752	0.683	0.673	0.53	0.222	0.153	0.143	0.00167	0.00115	0.00108
3La	0.733	0.763	0.671	0.53	0.203	0.233	0.141	0.00153	0.00175	0.00106

Calculation of Absorbance and Drug Concentration Loading of Cephalexin

Sample	First Draw			Blanc	Abs 1	Abs 2	Abs3	Gentamicin releasing		
	Sample1	Sample2	Sample3	Blanc	Abs 1	Abs 2	Abs3	Conc1	Conc2	Conc3
CS	0.758	0.804	0.693	0.53	0.228	0.274	0.163	0.00172	0.00206	0.00123
1La	0.683	0.671	0.693	0.53	0.153	0.141	0.163	0.00115	0.00106	0.00123
2La	0.705	0.633	0.633	0.53	0.175	0.103	0.103	0.00132	0.00078	0.00078
3La	0.682	0.717	0.621	0.53	0.152	0.187	0.091	0.00115	0.00141	0.00069
Sample	Second draw			Blanc	Abs1	Abs 2	Abs 3	Gentamicin releasing		
	Sample1	Sample2	Sample3	Blanc	Abs 1	Abs 2	Abs 3	Conc1	Conc2	Conc3
CS	0.746	0.793	0.689	0.53	0.216	0.263	0.159	0.00163	0.00198	0.0012
1La	0.675	0.665	0.684	0.53	0.145	0.135	0.154	0.00109	0.00102	0.00116
2La	0.695	0.624	0.625	0.53	0.165	0.094	0.095	0.00124	0.00071	0.00072
3La	0.676	0.705	0.616	0.53	0.146	0.175	0.086	0.0011	0.00132	0.00065
Sample	Second draw			Blanc	Abs 1	Abs 2	Abs 3	Gentamicin releasing		
	Sample1	Sample2	Sample3	Blanc	Abs 1	Abs 2	Abs 3	Conc1	Conc2	Conc3
CS	0.738	0.781	0.676	0.53	0.208	0.251	0.146	0.00157	0.00189	0.0011
1La	0.669	0.658	0.678	0.53	0.139	0.128	0.148	0.00105	0.00097	0.00112
2La	0.581	0.615	0.617	0.53	0.051	0.085	0.087	0.00039	0.00064	0.00066
3La	0.665	0.694	0.603	0.53	0.135	0.164	0.073	0.00102	0.00124	0.00055

APPENDIX C.

CALCULATION THE DRUG PER MOL/L

Calculation the Drug mol/L of Ampicillin Loading

Slope equation	Samples	Abs 1.day	Abs 2.day	Abs 3.day	Drug mol/L1	Drug mol/L2	Drug mol/L3
y = 59.605x0.0015	CS	0.002201	0.001848	0.001625	0.000062	0.000056	0.000052
	1La:CS	0.002106	0.001865	0.001669	0.00006	0.000056	0.000053
	2La:CS	0.002245	0.002106	0.001988	0.000063	0.00006	0.000059
	3La:CS	0.002357	0.002324	0.002038	0.000065	0.000064	0.000059

Calculation The Drug mol/L of Ampicillin Releasing

Slope equation	Samples	Abs 1.day	Abs 2.day	Abs 3.day	Drug mol/L1	Drug mol/L2	Drug mol/L3
y = 59.605x-0.0015	CS	0.001434	0.001289	0.001149	4.92E-05	4.68E-05	0.0000444
	1La:CS	0.001518	0.001177	0.000998	5.06E-05	4.49E-05	0.0000419
	2La:CS	0.001781	0.001664	0.001429	5.50E-05	5.31E-05	0.0000491
	3La:CS	0.001871	0.001703	0.001524	5.66E-05	5.37E-05	0.0000507

Calculation the Drug mol/L of Gentamicin Loading

Slope equation	Samples	Abs 1.day	Abs 2.day	Abs 3.day	Drug mol/L1	Drug mol/L2	Drug mol/L3
y = 216.34x-0.0102	CS	0.0006231	0.0005707	0.0005322	2.88E-06	2.64E-06	2.46E-06
	1La:CS	0.0006693	0.0006416	0.0006246	3.09E-06	2.97E-06	2.89E-06
	2La:CS	0.0006863	0.0006431	0.0006077	3.17E-06	2.97E-06	2.81E-06
	3La:CS	0.0006986	0.0006554	0.0006293	3.23E-06	3.03E-06	2.91E-06

Calculation the Drug mol/L of Gentamicin Releasing

Slope equation	Samples	Abs 1.day	Abs 2.day	Abs 3.day	Drug mol/L1	Drug mol/L2	Drug mol/L3
y = 216.34x-0.0102	CS	0.0004228	0.0003904	0.0003458	1.95E-06	1.80E-06	1.60E-06
	1La:CS	0.0004798	0.0004474	0.0004043	2.22E-06	2.07E-06	1.87E-06
	2La:CS	0.0004798	0.0004182	0.0003796	2.22E-06	1.93E-06	1.75E-06
	3La:CS	0.0004829	0.0004336	0.0003874	2.23E-06	2.00E-06	1.79E-06

Calculation the Drug mol/L of Cephalexin Loading

Slope equation	Samples	Abs 1.day	Abs 2.day	Abs 3.day	Drug mol/L1	Drug mol/L2	Drug mol/L3
y = 133.35x-0.001	CS	0.002145	0.002012	0.001955	2.36E-05	2.26E-05	2.22E-05
	1La:CS	0.001612	0.001552	0.001467	1.96E-05	1.91E-05	1.85E-05
	2La:CS	0.001415	0.001367	0.001302	1.81E-05	1.76E-05	1.73E-05
	3La:CS	0.001575	0.001505	0.001450	1.93E-05	1.88E-05	1.84E-05

Calculation the Drug mol/L of Cephalexin Releasing

Slope equation	Samples	Abs 1.day	Abs 2.day	Abs 3.day	Drug mol/L1	Drug mol/L2	Drug mol/L3
y = 133.35x-0.001	CS	0.001670	0.001602	0.001520	2.00E-05	1.95E-05	1.89E-05
	1La:CS	0.001150	0.001092	0.001045	1.61E-05	1.57E-05	1.53E-05
	2La:CS	0.000960	0.000892	0.000565	1.47E-05	1.42E-05	1.17E-05
	3La:CS	0.001082	0.001025	0.000937	1.56E-05	1.52E-05	1.45E-05

APPENDIX D.

CALCULATION THE MASS PER GRAM

Calculation The Mass Per Gram of Ampicillin Loading

Samples	Molarity of drug 1	Molarity of drug 2	Molarity of drug 3	Molecular Weight	Volume (L)	Mass(gram) for drug loading		
CS	6.20921E-05	5.617E-05	5.243E-05	371.39	0.02	1.1530	1.0430	0.9736
1La:CS	6.04983E-05	5.6455E-05	5.317E-05	371.39	0.02	1.1234	1.0483	0.9873
2La:CS	6.28303E-05	6.050E-05	5.852E-05	371.39	0.02	1.1667	1.1234	1.0867
3La:CS	6.47093E-05	6.416E-05	5.936E-05	371.39	0.02	1.2016	1.1913	1.1022

Calculation The Mass Per Gram of Ampicillin Releasing

Samples	Molarity of drug 1	Molarity of drug 2	Molarity of drug 3	Molecular Weight	Volume (L)	Mass(gram) for drug loading		
CS	4.92241E-05	4.679E-05	4.444E-05	371.39	0.02	0.9141	0.8689	0.8253
1La:CS	5.06333E-05	4.491E-05	4.191E-05	371.39	0.02	0.9402	0.8340	0.7782
2La:CS	5.50457E-05	5.308E-05	4.914E-05	371.39	0.02	1.0222	0.9857	0.9125
3La:CS	5.65557E-05	5.374E-05	5.0734E-05	371.39	0.02	1.0502	0.9979	0.9421

Calculation The Mass per Gram of Gentamicin Loading

Samples	Molarity of drug 1	Molarity of drug 2	Molarity of drug 3	Molecular Weight	Volume (L)	Mass(gram) for drug loading		
CS	2.8802E-06	2.6380E-06	2.4600E-06	692.93	0.01	0.1996	0.1828	0.1705
1La:CS	3.0938E-06	2.9656E-06	2.8873E-06	692.93	0.01	0.2144	0.2055	0.2001
2La:CS	3.1722E-06	2.9727E-06	2.8089E-06	692.93	0.01	0.2198	0.2060	0.1946
3La:CS	3.2291E-06	3.0297E-06	2.9086E-06	692.93	0.01	0.2238	0.2099	0.2015

Calculation The Mass Per Gram of Gentamicin Releasing

Samples	Molarity of drug 1	Molarity of drug 2	Molarity of drug 3	Molecular Weight	Volume (L)	Mass(gram) for drug loading		
CS	1.954E-06	1.8047E-06	1.510E-06	692.93	0.01	0.1354	0.1251	0.1107
1La:CS	2.218E-06	2.0682E-06	1.869E-06	692.93	0.01	0.1537	0.1433	0.1295
2La:CS	2.218E-06	1.9329E-06	1.755E-06	692.93	0.01	0.1537	0.1339	0.1216
3La:CS	2.232E-06	2.0041E-06	1.791E-06	692.93	0.01	0.1547	0.1389	0.1241

Calculation The Mass Per Gram of Cephalexin Loading

Samples	Molarity of drug 1	Molarity of drug 2	Molarity of drug 3	Molecular Weight	Volume (L)	Mass(gram) for drug loading		
CS	2.358E-05	2.2589E-05	2.2158E-05	347.39	0.014	0.5852	0.5605	0.5498
1La:CS	1.959E-05	1.9140E-05	1.8503E-05	347.39	0.014	0.4861	0.4749	0.4591
2La:CS	1.811E-05	1.7753E-05	1.7265E-05	347.39	0.014	0.4493	0.4405	0.4284
3La:CS	1.931E-05	1.8784E-05	1.8371E-05	347.39	0.014	0.4791	0.4661	0.4559

Calculation the mass per gram of cephalexin releasing

Samples	Molarity of drug 1	Molarity of drug 2	Molarity of drug 3	Molecular Weight	Volume (L)	Mass(gram) for drug loading		
CS	2.002E-05	1.9515E-05	1.8896E-05	347.39	0.014	0.4968	0.4842	0.4689
1La:CS	1.612E-05	1.5691E-05	1.5335E-05	347.39	0.014	0.4000	0.3893	0.3805
2La:CS	1.470E-05	1.4191E-05	1.1736E-05	347.39	0.014	0.3647	0.3521	0.2912
3La:CS	1.562E-05	1.5185E-05	1.4529E-05	347.39	0.014	0.3875	0.3768	0.3605